

1 **Assessment of variability of the thermohaline structure and transport of**
2 **Atlantic water in the Arctic Ocean based on NABOS CTD data**

3 Nataliya Zhurbas¹ and Natalia Kuzmina¹

4 ¹Shirshov Institute of Oceanology, Russian Academy of Sciences, 36 Nakhimovsky Prospekt ,
5 117997 Moscow, Russia

6 *Correspondence to:* Nataliya Zhurbas (nvzhurbas@gmail.com)

7

8 **Abstract.** Data of CTD transects across continental slope of the Eurasian Basin and the St. Anna
9 Trough performed during NABOS (Nansen and Amundsen Basins Observing System) project in
10 2003–2015 **are** used to assess transport and propagation features of the Atlantic Water (AW) in
11 the Arctic Ocean. Estimates of θ - S **indices** and volume flow rate of the current carrying the AW
12 in the Eurasian Basin **were** obtained. The assessments were based on the analysis of CTD data
13 including 33 sections in the Eurasian Basin, 4 transects in the St. Anna Trough and 2 transects in
14 the Makarov Basin; additionally a CTD transect of the PolarStern-1996 expedition (PS-96) was
15 considered. Using spatial distributions of temperature, salinity, and density on the transects and
16 applying θ - S analysis, the variability of thermohaline pattern on the AW pathway along the slope
17 of Eurasian Basin was investigated. The Fram Strait branch of the Atlantic Water (FSBW) was
18 ~~satisfactorily~~ identified on all transects, including two transects in the Makarov Basin (along
19 159°E), while the cold waters, which can be associated with the influence of the Barents Sea
20 branch of the Atlantic water (BSBW), on the transects along 126°E, 142°E and 159°E, were
21 observed in the depth range below 800 m and had a negligible effect on the spatial structure of
22 isopycnic surfaces. Special attention was paid to the variability of the volume flow rate of the
23 AW propagating along the continental slope of the Eurasian Basin. The geostrophic volume flow
24 rate was calculated using the dynamic method. An interpretation of the spatial and temporal
25 variability of hydrological parameters characterizing the flow of the AW in the Eurasian Basin is
26 presented. The geostrophic volume flow rate decreases significantly farther away from the areas
27 of the AW inflow to the Eurasian Basin. Thus, the geostrophic estimate of the volume rate for
28 the AW flow in the Makarov Basin at 159°E was found to be more than an order of magnitude
29 smaller than the estimates of the volume flow rate in the Eurasian Basin, implying that the major
30 part of the AW entering the Arctic Ocean circulates cyclonically within the Nansen and
31 Amundsen Basins. There is an absolute maximum of θ_{max} (AW core temperature) in 2006–2008
32 time series and a maximum in 2013, but only at 103°E. Salinity $S(\theta_{max})$ (AW core salinity) time
33 series display an increase of the AW salinity in 2006–2008 and 2013 (at 103°E) that can be
34 referred to as a AW salinization in the early 2000-ies. The maxima of θ_{max} and $S(\theta_{max})$ in 2006-
35 2008 and 2013 were accompanied by the volume flow rate highs. **Additionally the time average**
36 **volume rates were calculated for the FSBW flow** (in the longitude range 31–92°E), for the
37 BSBW flow in the St. Anna Trough and for a combined FSBW and BSBW flow in longitude
38 range 94–107°E. **A detailed discussion of the results is presented.**

39 1. Introduction

40 It is well known (see, e.g., Aagaard, 1981; Rudels et al., 1994; Schauer et al., 1997; Rudels
41 et al., 1999; Schauer et al., 2002; Rudels et al., 2006; Berzczynska-Möller et al., 2012; Rudels et

42 al., 2015; Rudels, 2015; Dmitrenko et al., 2015) that Atlantic water (AW) enters the Eurasian
43 Basin in two ways: one part originates from the Greenland and Norwegian seas and flows to the
44 Basin through the Fram Strait (Fram Strait branch of the Atlantic Water, hereinafter the FSBW
45 in accordance with the terminology of the paper by Schauer et al. (1997)), and the other reaches
46 the deep part of the Arctic Ocean near St. Anna Through after passing through the Barents Sea
47 (Barents Sea branch of the Atlantic water, hereinafter the BSBW as in (Schauer et al., 1997)).
48 After entering the Eurasian Basin the FSBW forms an eastward subsurface baroclinic boundary
49 current with a core of increased temperature and salinity adjacent to the continental slope. In the
50 longitude range of 80–90°E it encounters and partially mixes with the BSBW, which is strongly
51 cooled due to mixing with shallow waters of the Arctic shelf seas. Further, the water masses
52 resulting from the interaction of two branches which transport the AW continue spreading
53 cyclonically in the Eurasian Basin, following the sea bed topography.

54 To study the characteristics of the FSBW and BSBW flow in the Eurasian Basin, it is
55 useful to estimate, first of all, its volume flow rate in different parts of the Basin. Generally the
56 estimates of the AW volume flow rate have been based on observationally derived velocities
57 (Fahrbach et al., 2001; Pnyushkov et al., 2011; Berzczynska-Möller et al., 2012; Rudels et al.,
58 2014). However, to solve a number of fundamental and climatic problems it is worth considering
59 the AW volume flow rate calculated on the basis of geostrophic (density-driven) velocity
60 estimates. Such estimates can be more close to the real average estimates of the baroclinic
61 volume flow rate since the velocity field in the ocean, in particular due to the internal waves and
62 inertial oscillations, is usually more variable than the temperature, salinity and density fields.

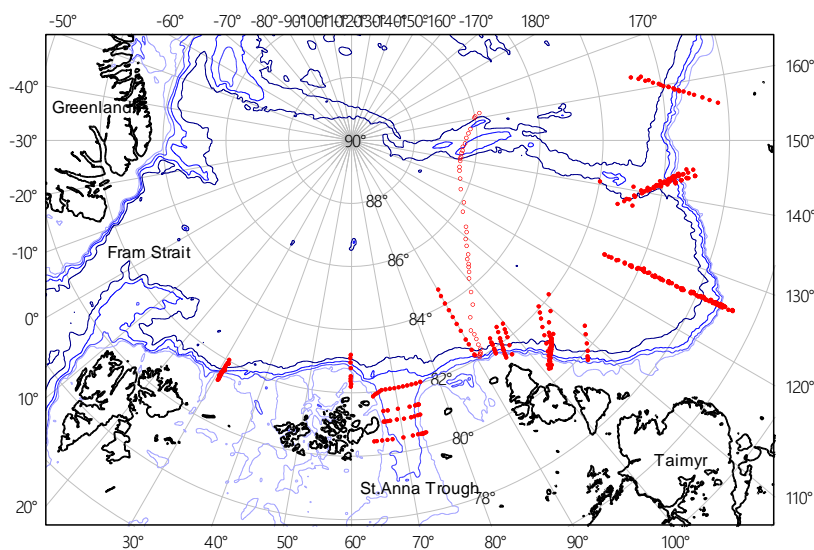
63 To estimate the volume flow rate and thermohaline parameters of the AW, a large amount
64 of CTD data is required. Obviously, the more complete the set of the considered sections the
65 more accurate would be the estimates. Within the **NABOS project** (Nansen and Amundsen
66 Basins Observing System) a unique array of CTD data was collected: more than 30 sections were
67 made in various regions of the Arctic Basin in the years 2002–2015. Moreover, a number of
68 sections in different years were made in the same regions of the Basin, which allows studying the
69 temporal interannual variability of the thermohaline structure of water masses in these areas.

70 The main goal of this work is to investigate the spatial and temporal variability of the AW
71 volume flow rate during its propagation along the continental slope of the Eurasian Basin using
72 geostrophic estimates. Another important aspect of our analysis is the investigation of the
73 thermohaline structure of the FSBW and BSBW and of its transformation. Large array of CTD
74 data obtained using the NABOS program in 2002–2015 is used to get the results.

75 2. Material and Methods

76 In this study we used data of CTD profiling on transects across the slope of the Eurasian
 77 Basin in the longitude range of 31–159°E measured in the years 2002–2015 within the
 78 framework of NABOS project (in total 39 transects). The data are freely available at the site
 79 <http://nabos.iarc.uaf.edu>. Apart from the NABOS data, a famous CTD transect across the whole
 80 Eurasian Basin and over the Lomonosov Ridge starting at 92°E at the slope from R/V *Polarstern*
 81 in 1996 (hereafter PS96) was also included. The location of the CTD transects is shown in Fig. 1.
 82 It can be seen from the map in Fig. 1 that most of the CTD transects are aligned cross-slope and
 83 grouped at longitudes of 31, 60, 90, 92, 94, 96, 98, 103, 126, 142, and 159°E. Four of the 40
 84 transects crossed zonally the St. Anna Trough (at the latitude of 81, 81.33, 81.42, and 82°N)
 85 through which the ~~Barents Sea Branch of the Atlantic Water (BSBW)~~ enters the Eurasian Basin.
 86 Most of the CTD casts covered the upper layer from the sea surface to either 1000 m depth or to
 87 the bottom (if the ~~depth of the sea~~ was less than 1000 m); some of the CTD casts (approximately
 88 every third or fourth) covered the depths from the sea surface down to the sea bottom even if the
 89 sea depth exceeded 1000 m.

90



91

92 Fig.1. Bathymetric map of the Eurasian Basin with 300, 500, 1000, and 2000 m contours shown.
 93 The red filled and blank circles are the locations of CTD stations on the NABOS and PS96
 94 transects, respectively.

95 To estimate the strength of the ~~Fram Strait branch (FSBW)~~ or the ~~Barents Sea branch~~
 96 ~~(BSBW)~~ or both branches of the Atlantic Water, we applied **classical geostrophic relations**

$$97 \quad \frac{\partial u}{\partial z} = \frac{g}{f\rho_0} \frac{\partial \rho}{\partial y}, \quad \frac{\partial v}{\partial z} = -\frac{g}{f\rho_0} \frac{\partial \rho}{\partial x}, \quad (1)$$


98 where u and v are velocity components along the x and y axes, respectively, g is the gravity
 99 acceleration, f is the Coriolis parameter, and ρ and ρ_0 are the density and reference density,
 100 respectively; x, y, z is the right-hand triplet of orthogonal axes (e.g., the x , y , and z axes are
 101 directed east, north, and upward, respectively).

102 The choice of such a coordinate system is convenient for the stated task. Indeed,
 103 assuming that the direction of the flow which transports AW is perpendicular to the transects
 104 (that is, the flow is directed strictly along the slope), the first equation of Eqs. (1) was used to
 105 calculate the flow velocity in the Eurasian basin. The second equation of Eqs. (1) was used to
 106 estimate the flow velocity in the St. Anna Through.

107 The horizontal gradients of density, $\partial\rho/\partial x$ or $\partial\rho/\partial y$, can be estimated from CTD
 108 measurements (non-averaged data) on the transect providing the possibility to calculate vertical
 109 gradients of velocity, $\partial v/\partial z$ or $\partial u/\partial z$ by Eqs. (1) and finally assess velocities u and v by
 110 vertical integration.

111 The horizontal density gradients were determined on the basis of primary, **non-averaged**
 112 CTD data, after which the vertical velocity gradients were calculated based on Eqs. (1), and then
 113 the velocity values $u(z, y)$ were obtained by vertical integration.

114 The main problem with geostrophic estimates of velocity from CTD transects lies in the
 115 **uncertainty of choice of the no motion level** (the zero velocity depth ~~or the reference horizon~~). If
 116 one expects that the baroclinic current occupies the upper layer or/and some intermediate layer
 117 while the deep layer is relatively calm, the no motion depth level (or the reference horizon) can
 118 be chosen somewhere in a supposedly calm deep layer (where the horizontal density gradient is
 119 very small). On the contrary, in case of a near-bottom gravity flow, one would expect relative
 120 stillness in the overlying layers, so the no motion depth level can be reasonably chosen
 121 somewhere well above the near-bottom flow. The first situation is applicable to the FSBW,
 122 which is a near-surface current when entering the Eurasian Basin and is transformed to
 123 subsurface, intermediate-layer flow on its pathway along the slope of the Eurasian Basin. The
 124 latter situation is applicable to the BSBW in the St. Anna Trough. In view of the above
 125 considerations, we adopted for the no motion depth level either 1000 m depth or the sea bottom
 126 depth if the latter was smaller than 1000 m for the FSBW, and some level in the vicinity of 50 m
 127 depth, where density contours were more or less flat, for the observations of BSBW in the St.
 128 Anna Trough (see also below). An additional argument in favor of such a choice of the no
 129 motion depth level is that the CTD sections were made in the areas of Arctic Ocean covered with
 130 ice, and, consequently, the elevations of the free surface due to convergence/divergence caused
 131 by the heterogeneity of the Ekman wind transport, which could form the barotropic component

132 of the geostrophic flow,  absent: the ice cover extent of all sections, except for the
133 southernmost section in the Laptev Sea, at 126°E, was estimated to be about 95%.

134 Another problem with the geostrophic estimates of velocity from non-averaged CTD-data
135 is caused by vertical undulations of density contours on transect due to internal waves and
136 mesoscale eddies that can cause large fluctuations of horizontal density gradients and, therefore,
137 unrealistically high estimates of geostrophic velocities. The masking effect of internal waves and
138 mesoscale eddies on geostrophic estimates of velocity is especially important for transects with
139 closely spaced CTD casts, when the distance between neighbor casts is only a few kilometers
140 (this is our case). However, the masking effect of internal waves and mesoscale eddies can be
141 suppressed by integrating geostrophic velocities horizontally and vertically to get volume flow
142 rate through the CTD transect. Indeed, to get correct estimates of geostrophic velocities, it is
143 better not to use non-averaged data: it is useful to perform averaging and mapping the data on a
144 regular grid. Selecting the optimal smoothing and regular grid mapping parameters in each
145 specific case of a CTD section to determine geostrophic current velocities is beyond the scope of
146 this paper: here we only present estimates of the volume flow rate calculated on the basis of a
147 formal approach to the analysis of non-averaged CTD data which excludes the subjectivity of
148 choice of averaging and mapping parameters.

149 Since the FSBW brings saline and warm water to the Eurasian Basin, the geostrophic
150 estimates of the volume flow rate were found by integration over the depth range with positive
151 temperature, $\theta > 0$ °C, and relatively high salinity, $S > 34.5$ psu, that is, some areas in the near-
152 surface layer with warm and fresh water (which cannot be attributed to AW) were excluded. For
153 the observations of BSBW in the St. Anna Trough the geostrophic estimates of the volume flow
154 rate were found by integration over a depth range with the non-averaged temperature below 0 °C
155 and the salinity above 34.5 psu. If both branches of AW were present on the transect, the
156 integration was performed over the entire depth range except the cold near-surface layer ($\theta < 0$
157 °C) and the areas in the near-surface layer with warm ($\theta > 0$ °C) and relatively fresh ($S < 34.5$
158 psu) water. The zero velocity depth in this case was chosen in accordance to the observed pattern
159 of density contours, i.e. its resemblance with either the near-surface flow pattern or the near-
160 bottom flow pattern (see Section 3 for details). For density ρ in Eqs. (1), the in situ water density
161 depending on temperature, salinity and pressure was adopted. A detailed description of the
162 method for geostrophic estimates of the AW volume flow rate is presented in the paper (Zhurbas
163 N., 2019).

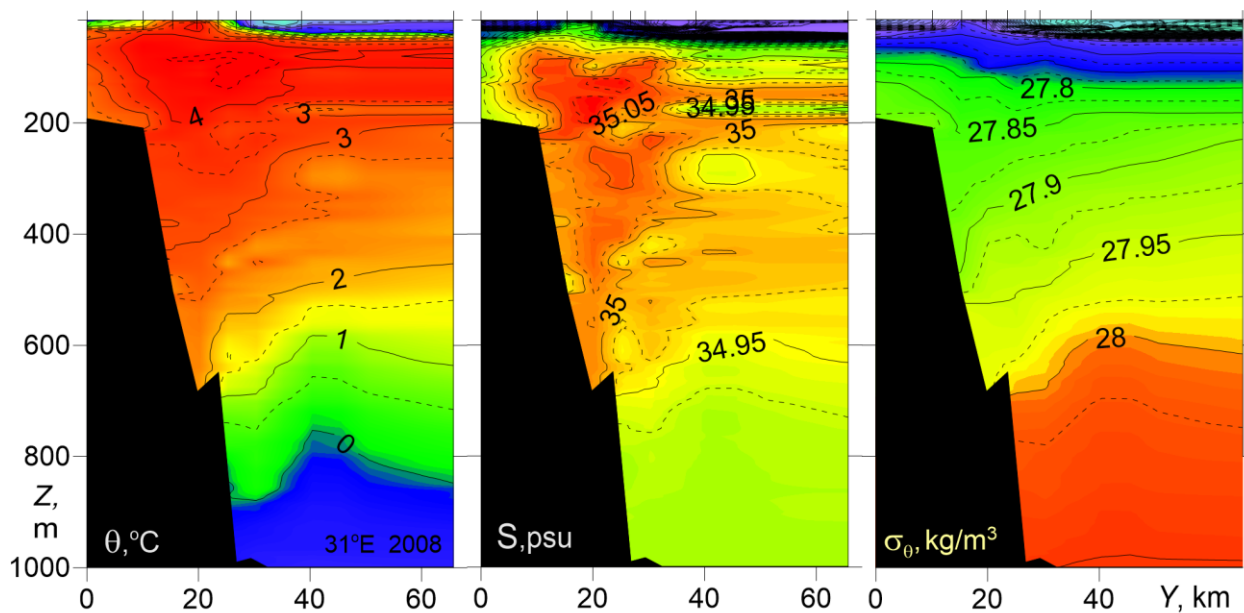
164 3. Results

165 3.1. Variability of the thermohaline pattern on the AW pathway along the slope of Eurasian 166 Basin

167 a. CTD transections analysis

168 First of all, let us focus on the transformation of thermohaline signatures (i.e. patterns of
169 salinity S , potential temperature θ , and potential density anomaly σ_θ , calculated relative to the
170 atmospheric pressure $p_0 = 0$ dbar, versus cross-slope distance and depth) of the AW flow on its
171 pathway along the slope of the Eurasian Basin. The potential density anomaly σ_θ pattern was of
172 primary interest, since it determines the geostrophic estimate of the AW transport (the values of
173 hydrological parameters and volume flow rates estimated for different areas of the AW flow
174 based on empirical data are presented in the table in Section 3.2).

175 **Fig. 2 shows** temperature, salinity, and potential density anomaly versus cross-slope
176 distance and depth from transect at 31°E, made in 2008. ~~As it can be seen in Fig. 2,~~ the contours
177 of σ_θ diverge towards the continental slope margin (to the south), shallowing above the
178 warm/saline core of the AW and sloping down beneath it, which in terms of geostrophic balance
179 corresponds to the eastward subsurface flow. Such a structural feature of the distribution of
180 isopycnic surfaces was observed on all NABOS transects taken across available continental
181 slope at 31°E. According to Fig. 2 the warm/saline core of the Fram Strait Branch of the AW
182 with the maximum temperature θ_{max} of 4.88°C at the depth $Z_{\theta_{max}}=102$ m and the maximum
183 salinity S_{max} of 35.11 **psu** at the depth $Z_{S_{max}}=176$ m is found on the slope at about 1000 m
184 isobath. It is obvious that the salinity maximum depth must be always larger than the
185 temperature maximum depth to satisfy the condition of hydrostatic stability. Indeed, if $Z_{\theta_{max}}=$
186 $Z_{S_{max}}$ then $\partial\sigma_\theta/\partial z = 0$ at $z = Z_{\theta_{max}} = Z_{S_{max}}$ (hydrostatically neutral stratification), and if $Z_{\theta_{max}}>$
187 $Z_{S_{max}}$ then $\sigma_\theta(Z_{\theta_{max}}) < \sigma_\theta(Z_{S_{max}})$ (hydrostatically unstable stratification).

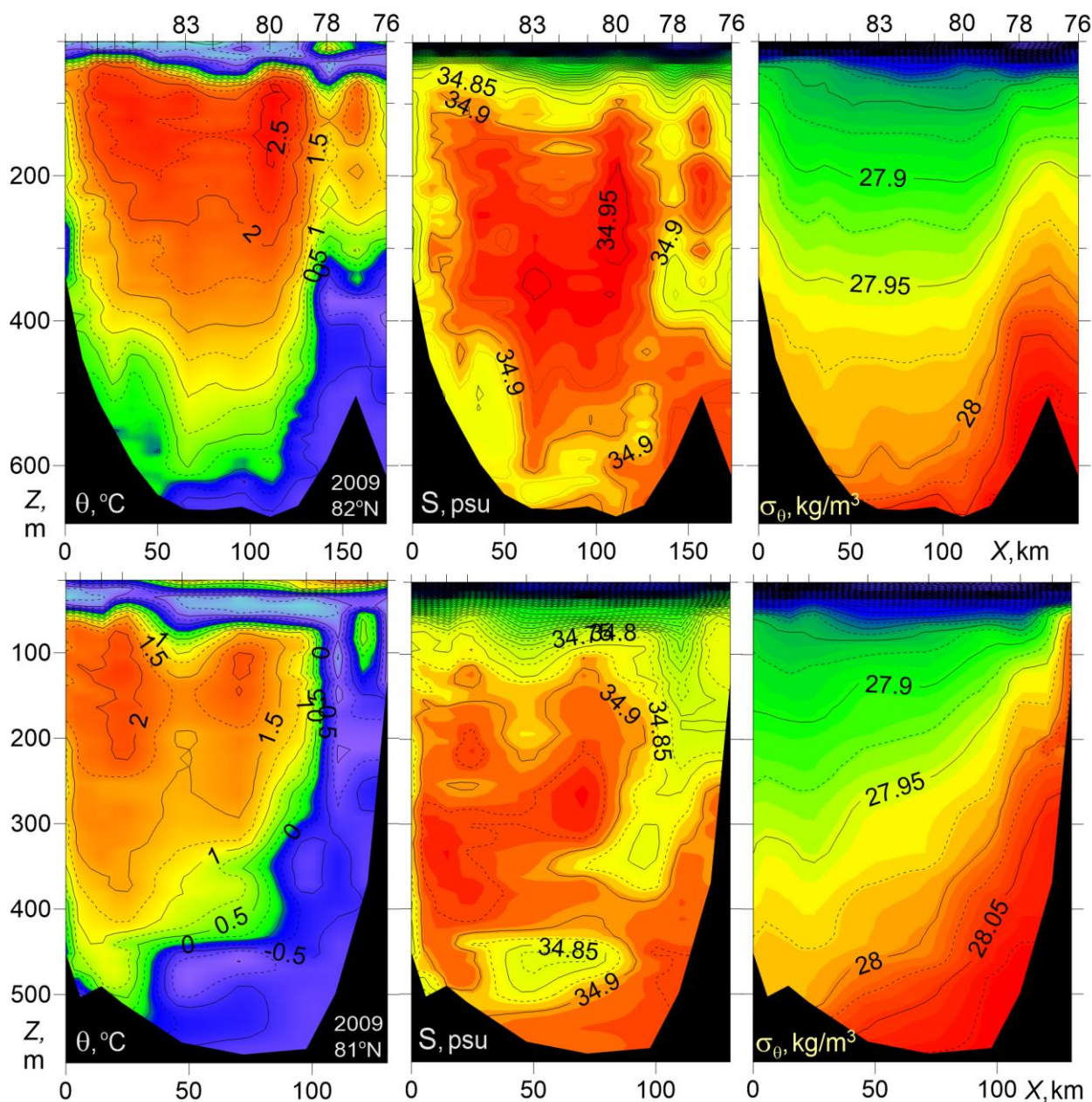


188

189 Fig. 2. Temperature θ , salinity S , and potential density anomaly σ_θ versus cross-slope distance
 190 and depth for the NABOS-2008 transect across the Eurasian Basin slope at 31°E.

191 Figure 3 presents temperature, salinity, and potential density versus distance and depth
 192 for two zonal transects across the St. Anna Trough at latitudes of 81 and 82°N. ~~These transects~~
 193 ~~presented in Fig. 3 are characterized by a stable pool of cold ($\theta < 0^\circ\text{C}$) and dense ($\sigma_\theta > 28 \text{ kg/m}^3$)~~
 194 water in the bottom layer adjacent to the eastern slope of the Trough. The transfer of the densest
 195 water pool to the eastern slope corresponds to a geostrophically balanced near-bottom gravity
 196 flow to the North. Note, that the gravity bottom currents are a typical feature of ocean dynamics
 197 and can develop in the narrows and troughs of various ocean basins (Arneborg et al., 2007;
 198 Zhurbas et al., 2012), so it is natural that the water flowing through St. Anna Trough in the
 199 Eurasian basin is transported **by a gravity current**. It is obvious that in case of near-bottom
 200 gravity current the no motion depth level for geostrophic calculations is implied to be well above
 201 the current. This near-bottom gravity current carries also waters of Atlantic origin, which are
 202 strongly cooled due to mixing with shallow waters of the Arctic shelf seas (the Barents and Kara
 203 seas). Above the near-bottom gravity flow of the BSBW one can observe two-core structure of
 204 warm FSBW with temperature up to 2.5 °C that enters the St. Anna Trough from the north-west
 205 at the western side of the Trough and leaves it for the north-east at the eastern side of the Trough.
 206 At 82°N (top panels in Fig. 3), the BSBW overflows a sufficiently deep ridge (at approx. 500 m
 207 depth) between the St. Anna Trough and the Voronin Trough. The latter is located in the
 208 longitude range of 80–90°E east of the St. Anna Trough and west of the Severnaya Zemlya
 209 islands (see Fig. 1). Therefore, one may suggest that a part of the BSBW enters the Eurasian
 210 Basin at 90°E leaving the Voronin Trough. ~~See also (Schauer et al., 2002; Rudels et al., 2014).~~

211

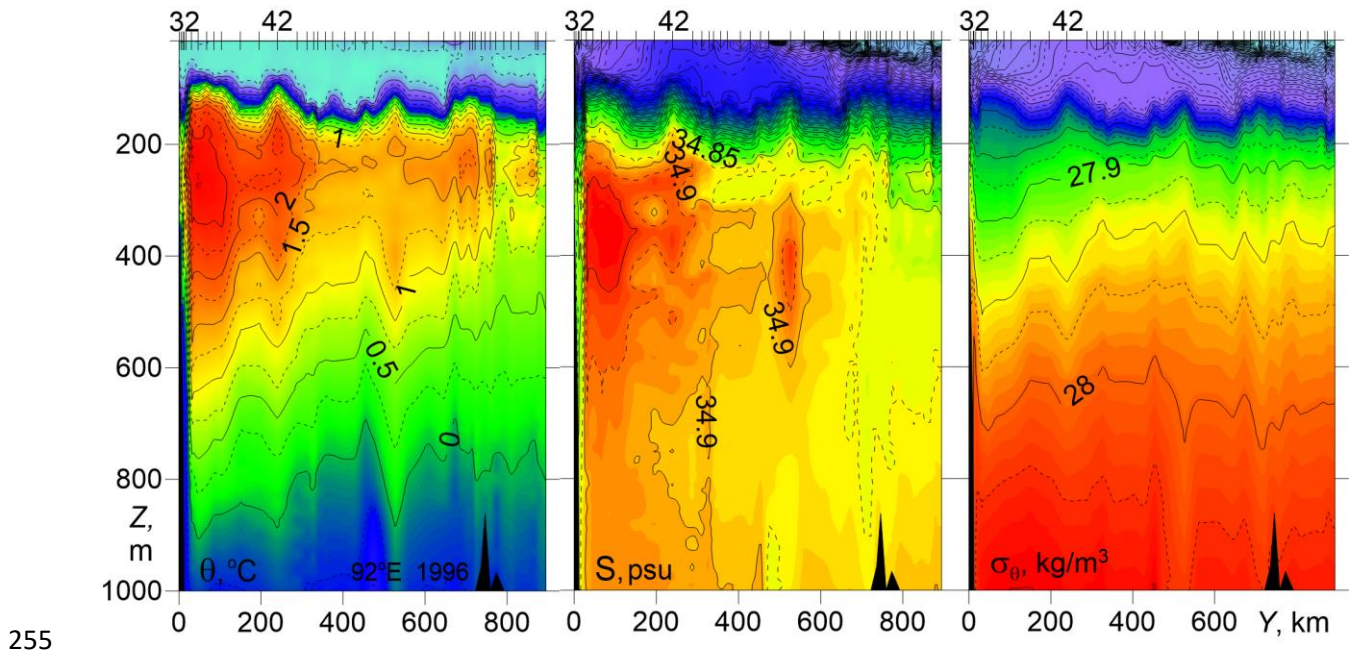
212
213

214 Fig. 3. Temperature θ , salinity S , and potential density anomaly σ_θ versus distance and depth for
 215 zonal transects across the St. Anna Trough at latitudes of 81°N (bottom, NABOS-2009), and
 216 82°N (top, NABOS-2009). The X -axis is directed to the east.

217 To understand the mechanisms of interaction and transformation of the FSBW and the
 218 BSBW, it is necessary to identify water masses of different origin. For that purpose the following
 219 criterion is often used (Walsh et al., 2007; Pfirman et al., 1994): the water masses of the FSBW
 220 are characterized by $\theta > 0$ °C, and the BSBW can be identified by the following expressions: -2
 221 °C $< \theta < 0$ °C, 34.75 psu $< S < 34.95$ psu and 27.8 kg/m³ $< \sigma_\theta < 28.0$ kg/m³. However, according to
 222 Fig. 3, the potential density σ_θ of the BSBW exceeds the upper limit of the last inequality,

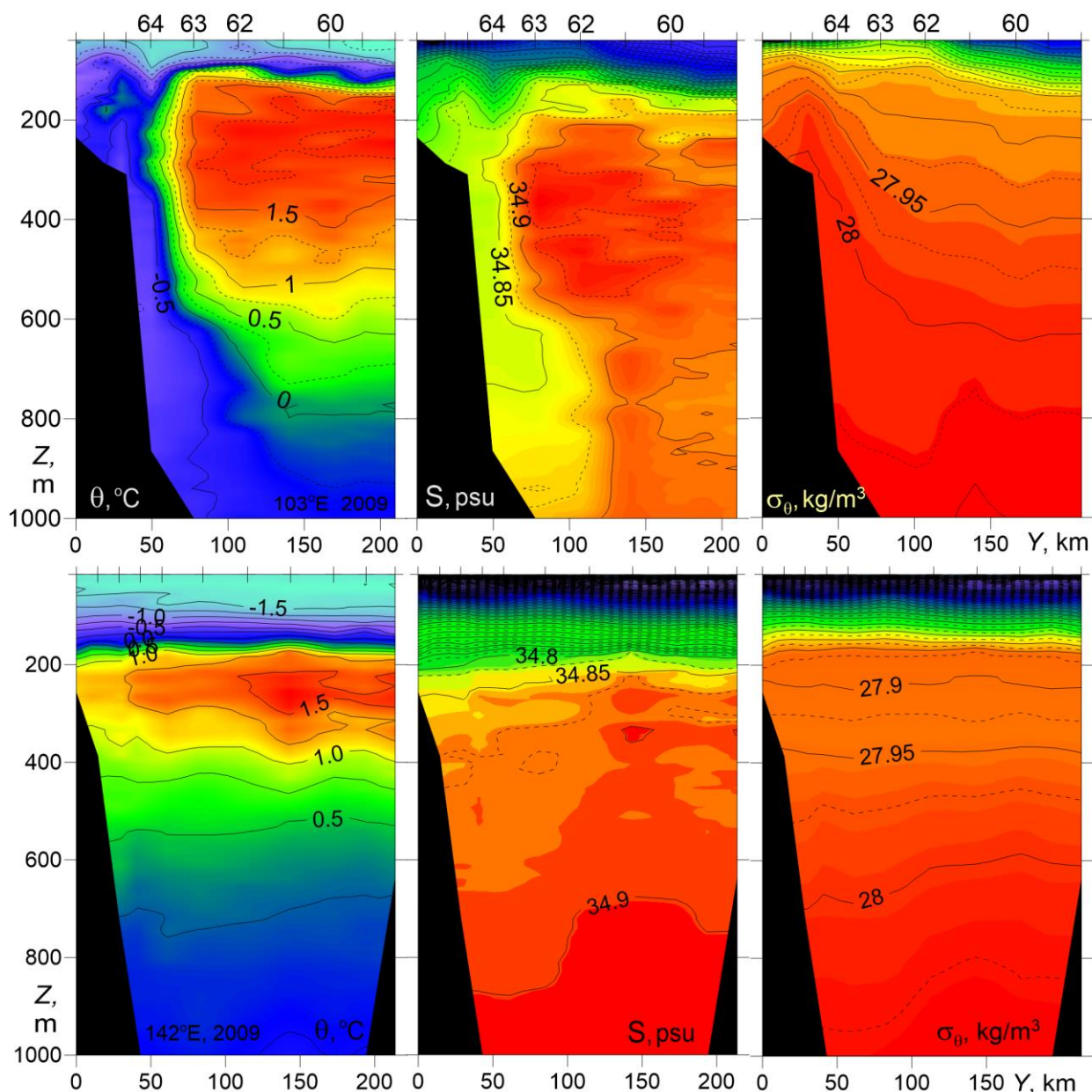
223 reaching the value of 28.05 kg/m^3 and the potential temperature θ does not reach the value of -2
 224 $^{\circ}\text{C}$ and is less than $-1 \text{ }^{\circ}\text{C}$ only in some cases. Thus, the BSBW thermohaline indices can be close
 225 to the values of temperature and salinity in the so-called Upper Polar Deep Water layer (UPDW,
 226 Rudels et al., 1994), the potential temperature of which lies within the range $-0.5 \text{ }^{\circ}\text{C} < \theta < 0 \text{ }^{\circ}\text{C}$,
 227 and the salinity is close to 34.9 psu (Walsh et al., 2007). Such a layer can be seen in Fig 2 in the
 228 depth range below 800 m . The overlapping of the ranges of variability of temperature and
 229 salinity for the UPDW and the BSBW makes it difficult to determine the origin of water masses
 230 in the eastern part of the Nansen Basin. In some cases, however, analysis of θ - S diagrams can
 231 provide useful information for identification of different water masses (see Subsection 3.1b).

232 In Fig. 4 the CTD transect at 92°E carried out in the *Polarstern*-1996 expedition just east of the
 233 entrance point of the BSBW to the Eurasian Basin from the St. Anna Trough and Voronin
 234 Trough is presented. It can be assumed that a part of the BSBW extends deep into the Basin,
 235 mixing with the FSBW, while another part of the BSBW moves eastward along the slope as a
 236 deep gravity current according to the general cyclonic circulation observed in the Eurasian
 237 Basin. On the presented transect the BSBW is observed in the depth range below 600 m as a
 238 narrow, about 10 km wide stripe of cold water near the slope (see also Subsection 3.1b) adjacent
 239 to a 300 km wide zone occupied by the warm FSBW. The pattern of the potential density of
 240 FSBW on this transect is similar to transects at 31°E . Namely, despite of the masking effect of
 241 vertical undulations of σ_{θ} contours caused by internal waves and mesoscale eddies (one of
 242 subsurface, intra-pycnocline eddies is probably identified at the distance of $Y=510 \text{ km}$), one
 243 cannot miss the tendency of shallowing/sloping down the σ_{θ} contours above/below the FSBW
 244 core towards the continental slope margin (to the south) which, in terms of geostrophic balance
 245 implies the eastward flow of FSBW. The FSBW core on the 92°E transect is found at 40 km
 246 distance from the slope, with the maximum temperature $\theta_{max}=2.79^{\circ}\text{C}$ at $Z_{\theta_{max}}=271 \text{ m}$ and
 247 salinity $S_{max}=34.97 \text{ psu}$ at $Z_{S_{max}}=329 \text{ m}$. Therefore, the FSBW on its pathway along the slope of
 248 the Eurasian Basin from 31°E to 92°E has cooled, desalinated, sank and become denser by
 249 approx. $2 \text{ }^{\circ}\text{C}$, 0.1 psu , 150 m , and 0.1 kg/m^3 , respectively. Another significant feature seen in the
 250 PS96 transect is an increased temperature pool in the layer of $180\text{--}300 \text{ m}$ at the distance of
 251 $Y=600\text{--}750 \text{ km}$ in the vicinity of the Lomonosov Ridge which can be attributed to the FSBW
 252 return flow cyclonically circulating around the Eurasian Basin. Note that the existence of return
 253 flow next to the Lomonosov Ridge is confirmed in terms of geostrophic balance by sloping down
 254 density contours towards Y -axis.



256 Fig. 4. Temperature θ , salinity S , and potential density anomaly σ_θ versus distance and depth for
 257 cross-shelf transects at 92°E (PS-1996).

258



259

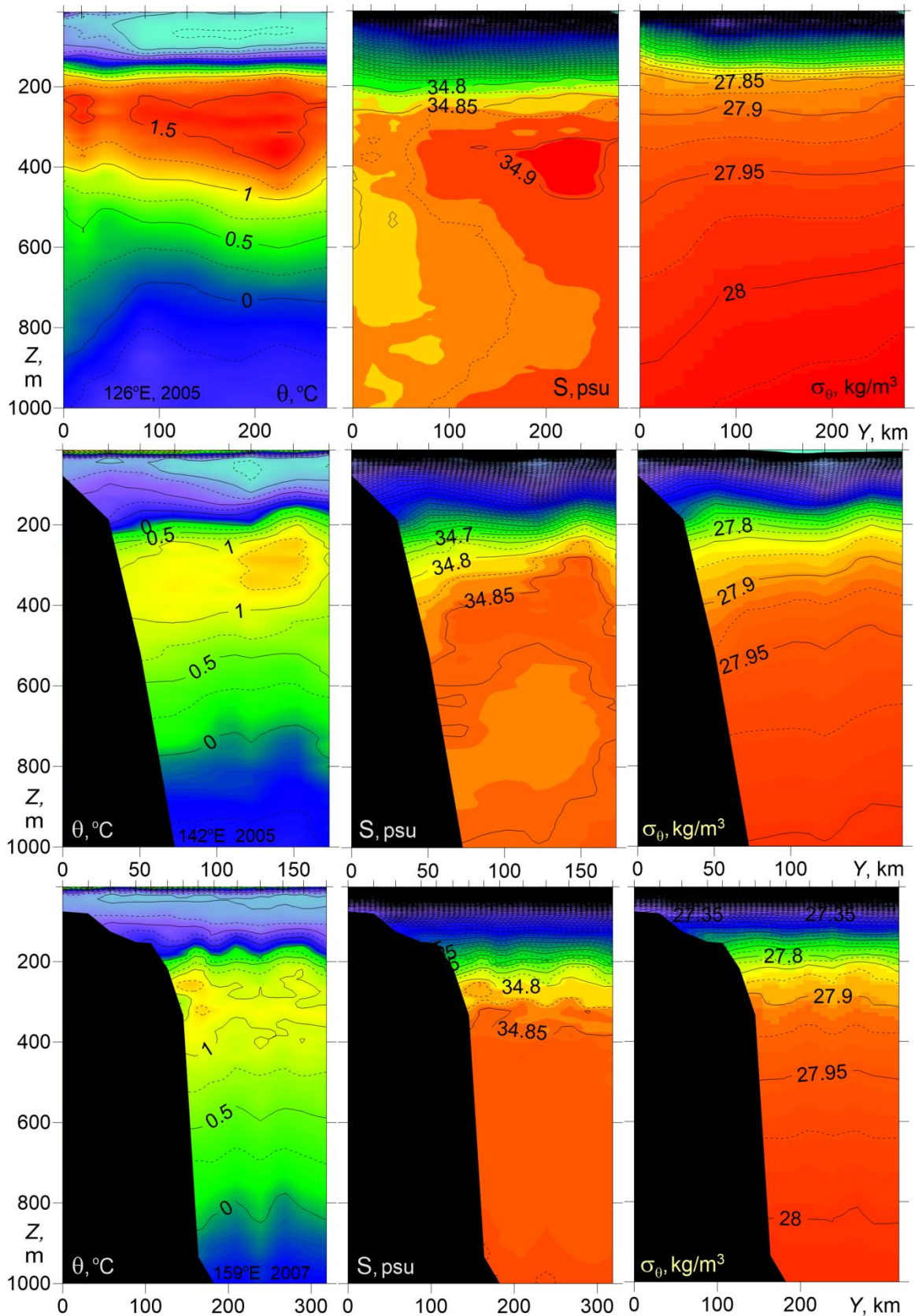
260 Fig. 5. Temperature θ , salinity S , and potential density anomaly σ_θ versus distance and depth for
 261 cross-shelf transects at 103°E (upper) and 142°E (lower) (NABOS-09).

262 Further east, in the longitude range of 94–107 °E (NABOS-09), the BSBW being denser dives
 263 under the FSBW, and the pattern of potential density on cross-slope transects is characterized by
 264 sloping down density contours towards the North in a 150 km wide zone adjacent to the slope
 265 (see Fig. 5, top panel) which is typical for the near-bottom gravity currents and corresponds to
 266 the eastward geostrophic flow provided that the no motion depth level remains within the above-
 267 lying layers. One reason to associate the BSBW with gravity current is the potential temperature
 268 values below -0.5 °C (see Subsection 3.1b). The vertical location of the FSBW layer has not
 269 changed much relative to the 92°E in the section PS-96 but the maximum temperature has further
 270 decreased: in the transect in Fig. 5, the top panel, $\theta_{max}=1.98$ °C at $Z_{\theta_{max}}=245$ m and $S_{max}=34.95$

271 psu at $Z_{Smax}=365$ m. The bottom panel of Fig. 5 presents the data from transect at 142°E
 272 (NABOS-09) which is located on the Lomonosov Ridge, the frontier between the Amundsen and
 273 Makarov Basins. The comparison of the two transects obtained in the same year shows that the
 274 vertical scale of the especially warm FSBW water ($\theta > 1.5$ °C) has significantly decreased.
 275 Nevertheless, it is obvious that the FSBW waters are also observed at these latitudes and affect
 276 the slopes of isopycnic surfaces in a layer up to 300 m. The cold waters with $\theta < 0$ °C, which can
 277 be associated with the BSBW, are observed only at two stations in the depth range close to 1000
 278 m, and are practically absent at the depths above 950 m. The slopes of isopycnic surfaces in the
 279 bottom panel of Fig. 5 are small, which is typical for weak geostrophic volume flow rate (see
 280 Section 3.2). It is worth noting that due to the low variability of the temperature and salinity
 281 fields, the water with ~~absolutely~~ stable thermohaline stratification is well visualized (Fig. 5,
 282 bottom panel): the temperature decreases and salinity increases with depth. This structural
 283 feature of the mean thermohaline stratification is also common to the UPDW (Rudels et al.,
 284 1999; Kuzmina et al., 2011, 2014).

285 In Fig. 6 three transects are presented, two of which were made at 126°E and 142°E
 286 (NABOS-2005) and the third one was made in the Makarov Basin at 159° E (NABOS-2007). On
 287 the transect along 126°E large slopes of isopycnic surfaces are observed, which corresponds to a
 288 fairly intensive geostrophic flow (see Section 3.2), confined to the depth range of 200–400 m,
 289 that is, to the area occupied by the FSBW. At the 142°E transect which is located on the
 290 Lomonosov Ridge, the frontier between the Amundsen and Makarov basins, and at the 159°E
 291 transect in the Makarov Basin, the FSBW **can be still identified as a warm layer** within a depth
 292 range of 200–400 m, where the maximum temperature has lowered to 1.49 °C and 1.42 °C,
 293 respectively (Fig. 6). One can observe **some sloping down** of potential density contours towards
 294 the continental slope on the 142°E transect implying some eastward geostrophic transport. As to
 295 the 159° E transect, the potential density contours **look quite flat, so one cannot visually identify**
 296 **any significant baroclinic flow**. In the area of cold waters (the depth range below 800 m) high
 297 slopes of isopycnic surfaces are not observed on any sections shown in Fig. 6, which may
 298 indicate the weakness or absence of the baroclinic flow.

299



300

301 Fig. 6. Temperature θ , salinity S , and potential density anomaly σ_θ versus distance and depth for
 302 cross-shelf transects at 126°E, 142°E (top and middle, NABOS-2005) and
 303 159°E (bottom, NABOS-2007).

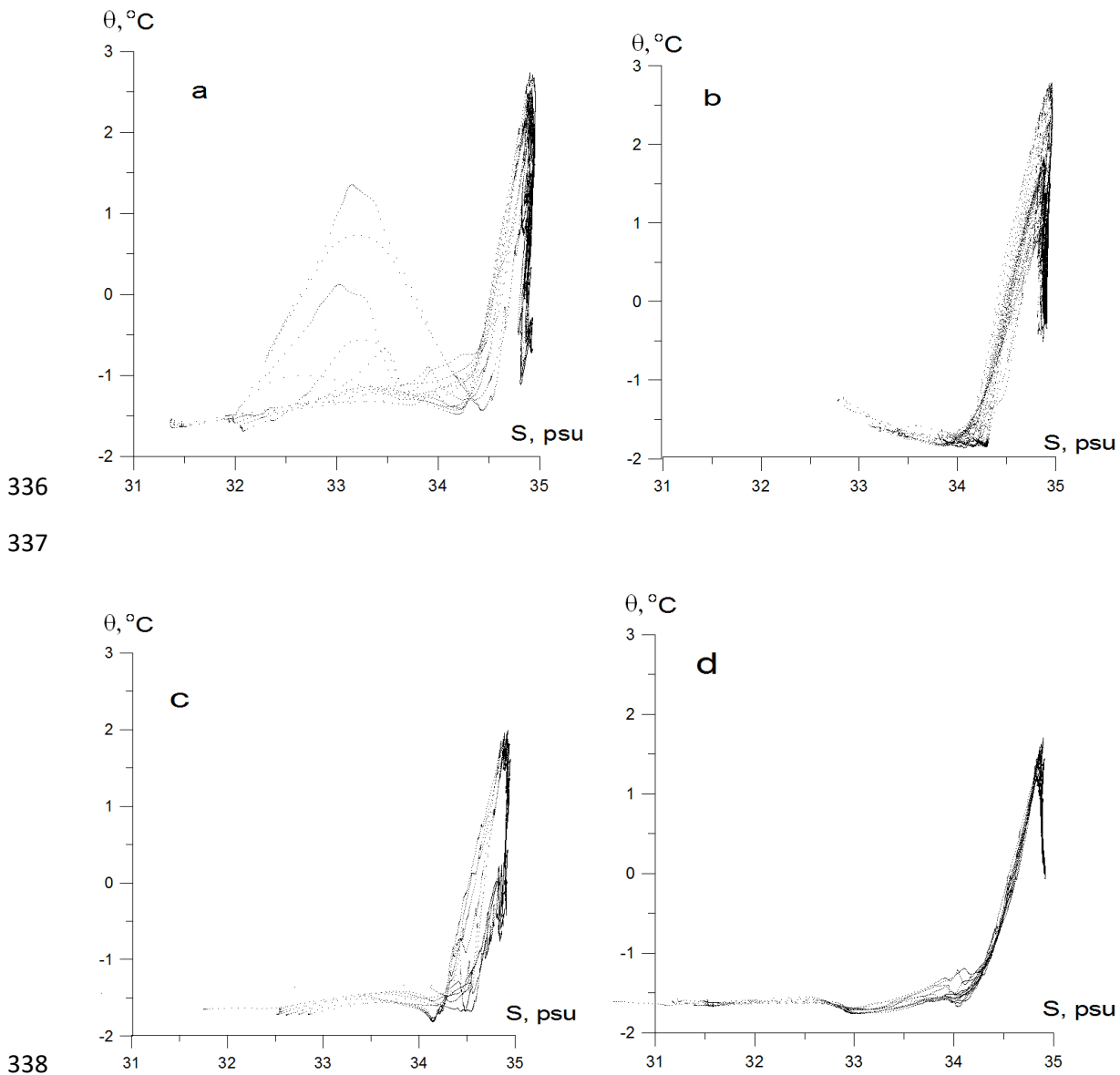
304 Concluding this section, we would like to state the following theses. The combined FSBW-
305 BSBW structure with isopycnals sloping down to the north (from the slope), is typical for the
306 longitude range 94–107°E. On the transects made along 126°E, 142°E, and 159°E, the slopes of
307 isopycnic surfaces indicating the baroclinic flow, were observed generally in the depth range of
308 200–400 m, that is in the area occupied by the FSBW. As the FSBW moved along the
309 continental slope of the Eurasian Basin, a significant decrease of temperature was observed in
310 the FSBW core. However, despite this the FSBW was satisfactorily identified at all transects,
311 including the two transects in the Makarov Basin (159°E). The cold waters on the transects along
312 126°E, 142°E and 159°E, which can be associated with the BSBW, had a minimum temperature
313 above -0.5 °C, were observed in the depth range below 800 m and had a little effect on the
314 spatial structure of isopycnic surfaces.

315 *b. θ -S analysis*

316 To study the transformation of various water masses in the Arctic Basin the θ -S analysis
317 have been applied in a number of papers (see, e.g., Schauer et al., 1997; Rudels et al., 1999;
318 Schauer et al., 2002; Rudels et al., 2004; Walsh et al., 2007; Dmitrenko et al., 2015). We will
319 also apply this method to study the transformation of BSBW along the slope.


320 ~~As mentioned above,~~ the difficulty in identifying the BSBW in the eastern part of the
321 Nansen Basin is related to the overlapping ranges of temperature and salinity inherent to the
322 BSBW and the upper layer of the Polar Deep Water (UPDW). It is also important to note that the
323 BSBW in the St. Anna Trough mixes with the FSBW. Therefore, not only the cold Atlantic
324 Waters, which are transported by the bottom gravity current, but also mixed warmer waters can
325 enter the Nansen Basin through the Trough (see Fig. 3). That is, one can observe some
326 resemblance in the potential temperature and salinity distributions across the St. Anna Trough
327 (Fig. 3) and that of the cross-slope section PS-96 at 92°E (Fig. 4), despite of the fact that the
328 CTD measurements were performed in different years. Therefore, it is expected that only a
329 detailed analysis of the θ -S indices on different CTD sections, obtained at approximately the
330 same time (e.g., the same year), can provide useful information on the movement and
331 transformation of BSBW.

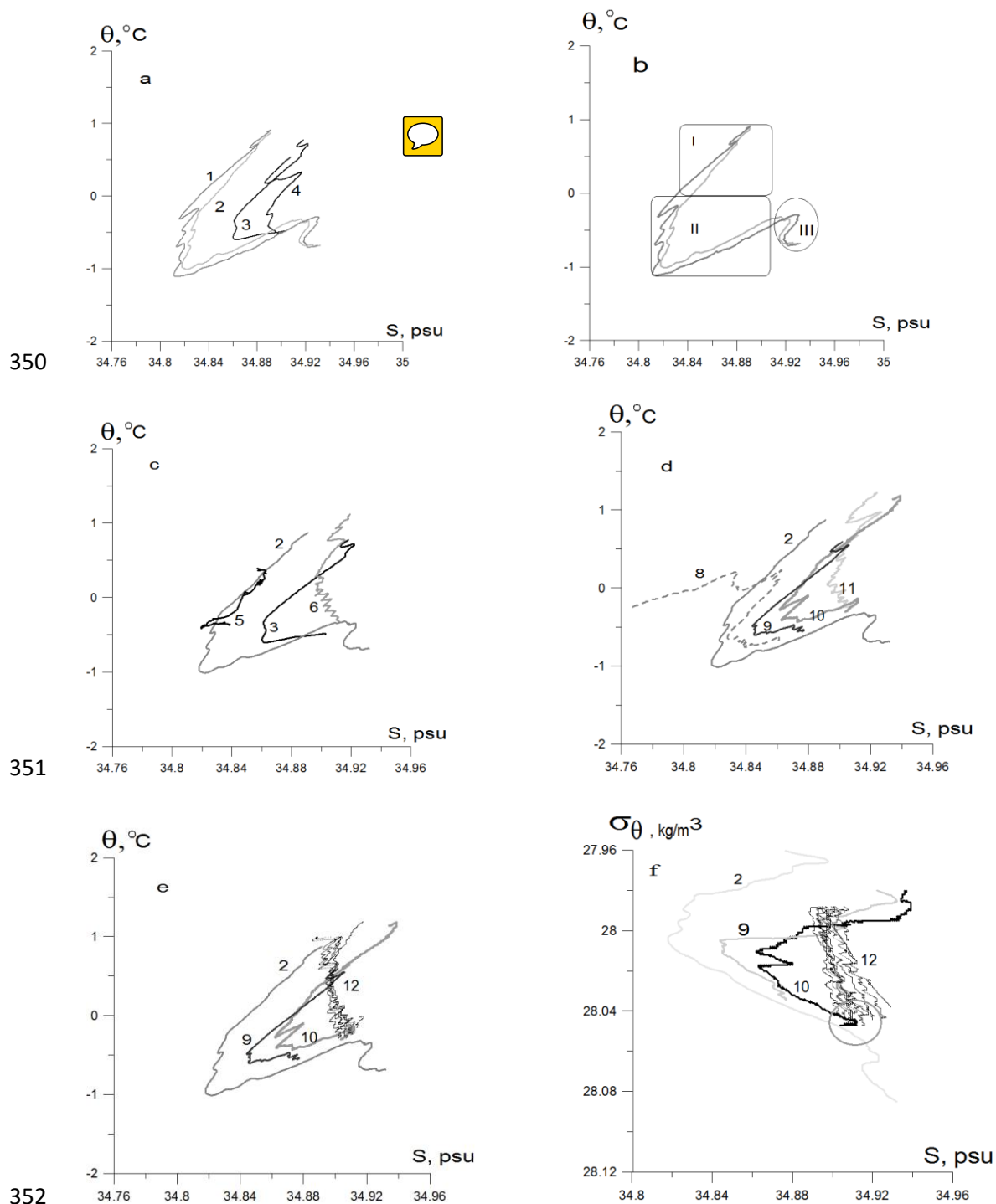
332 Fig. 7 presents θ -S diagrams based on the CTD profiling in (a) the St. Anna and Voronin
333 Troughs (NABOS-09, 82°N), (b) the PS-96 section at 92°E, and the NABOS-09 sections at
334 103°E (c) and 142°E (d). For convenience of presentation, the points of the θ -S curves with
335 salinity below 30 psu were omitted.



339 Fig. 7. θ - S diagrams based on the CTD profiling in (a) the St. Anna and Voronin troughs
 340 (NABOS-09, 82° N), (b) the PS-96 section at 92°E, and the NABOS-09 sections at 103°E (c)
 341 and 142°E (d).

342

343 ~~The diagrams presented in Fig. 7 have significant similarities and differences.~~  The
 344 differences in the behavior of the θ - S indices are observed in the upper and deep layers of the
 345 Eurasian Basin and the St. Anna Trough. On the other hand, one cannot miss a similarity in the
 346 shape of the θ - S curves in the salinity range of 34.5–35.0 psu. The similarity is obviously caused
 347 by the presence of FSBW. The plots in Fig. 7 demonstrate the transformation of the FSBW and
 348 BSBW moving along the continental slope of the Eurasian Basin. More detailed information on
 349 the BSBW transformation can be extracted from θ - S diagrams presented in Fig. 8.



353 Fig.8. Thermohaline indexes of the BSBW and FSBW: a) based upon the CTD profiles, obtained
 354 in the St. Anna Trough (NABOS-09, section 82°N), curves 1–4 correspond to the stations (st.)
 355 76, 78, 83 and 80, respectively; b) the same as “a” but only curves 1 and 2 are presented; regions
 356 I, II, III illustrate three different water masses in accordance with (Dmitrenko et al., 2015); for
 357 explanations see the text; c) based upon the section of PS-96, curves 5 and 6 corresponding to st.
 358 32 and 42, respectively (depth range 600–1000 m), curves 2 and 3 are shown for the reference;
 359 d) for CTD profiles at the 103°E section, NABOS-09, curve 8 (st. 64), curve 9 (st. 63), curve 10
 360 (st. 62), curve 11 (st. 60), and curve 2 for the reference (see Fig. 5 for the location of the
 361 stations); e) based upon the CTD profiles in the depth range 500–1200 m measured at the 126°E
 362 (section of NABOS-09), curves 12; curves 2, 9 and 10 are shown for the reference; f) the same
 363 as “e” but presented in coordinates σ_{θ} , S .

364 The θ - S diagrams related to the St. Anna Trough (NABOS-09, section 82°N) are presented
 365 in Fig. 8a. The curves marked as 1 and 2 correspond to stations 76 and 78, respectively, which
 366 were located at the eastern slope of the Trough just in the near-bottom gravity current carrying
 367 the BSBW, while the curves marked as 3 and 4 correspond to stations 83 and 80 located near the
 368 mid-point (thalweg) of the Trough in the western periphery of the gravity current (the location of
 369 the stations is shown in Fig. 3). To visualize better the BSBW transformation, the points of θ - S
 370 curves in the temperature and salinity ranges of $\theta > 1.2$ °C and $S < 34.76$ psu, respectively, were
 371 omitted. The same kind of similarity of the θ - S curves in the St. Anna Trough was observed
 372 within NABOS Program in other years (NABOS-13, NABOS-15).

373 The curves 1 and 2 in Fig. 8a have similar knee-like shape (Dmitrenko et al., 2015) formed
 374 by (i) the upper warm and saline water layer of the FSBW ($\theta \gg 0$ °C), (ii) the intermediate
 375 colder and fresher water layer of BSBW ($\theta < 0$ °C) underlying the FSBW, and (iii) the denser
 376 more warmer and saltier “true” mode of the BSBW ($\theta \approx 0$ °C). ~~To understand better the~~
 377 ~~differences between these water masses~~ see Fig. 8b: FSBW (region I), BSBW (region II), “true”
 378 mode BSBW (region III). The difference between the BSBW and “true” BSBW is in that the
 379 former is more diluted with the colder and fresher Barents Sea water (see paper by Dmitrenko et
 380 al. (2015) for more details). We will be interested in the transformation of the main part of the
 381 knee, namely the transformation of the moving along the slope BSBW.

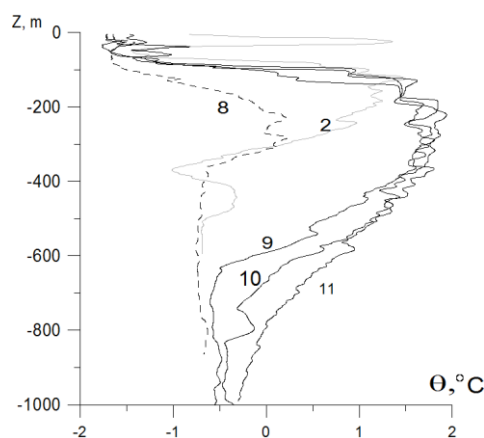
382 In Fig. 8c the comparison of typical θ - S curves related to the St. Anna trough (they are also
 383 shown in the other panels of Fig. 8 for reference) with that of the 92°E section of PS-96 is given:
 384 the curves 5 and 6 correspond to st. 32 and st. 42 (depth range 600–1000 m) of the PS-96
 385 section, respectively. St. 32 was located next to the slope, while st. 42 was located about 250 km
 386 apart from the slope. The coincidence of curve 5 with a part of curve 2 evidences for the BSBW
 387 moving along the slope in the form of a near-bottom gravity flow (see Fig. 4 and its legend 1).
 388 Curve 6 corresponds to the UPDW. The θ - S diagrams for CTD profiles at the section 103°E,
 389 NABOS-09, are given in Fig. 8d: curve 8 (st. 64), curve 9 (st. 63), curve 10 (st. 62), curve 11 (st.
 390 60), and the reference curve 2 (see Fig. 5 for the location of stations). Curves 8, 9, and 10 are
 391 similar to curve 2, and indicate the BSBW being an along-slope gravity flow. Curve 11, being
 392 similar to curve 6 in Fig. 8c, corresponds to the θ - S indices of the UPDW. However, the BSBW
 393 is not observed in the section 126°E: see Fig. 8e, where a bunch of θ - S curves (curves 12)
 394 presents all CTD profiles in the depth range 500–1200 m measured at the section 126°E of
 395 NABOS-09. Also we do not observe the BSBW further to the east on the section 142°E of
 396 NABOS-09 (not shown) as well as in the Makarov Basin.

397 To estimate the potential density of deep waters at the sections 103°E and 126°E σ_{θ} - S
 398 diagrams are shown in Fig. 8f: curves 2, 9 and 10 correspond to θ - S curves 2, 9 and 10 presented

399 in Fig. 8d, curves 12 correspond to curves 12 in Fig. 8e. As one can see, the BSBW is
 400 characterized by knee-shape diagram also in coordinates σ_θ, S . However the knee-shape diagram
 401 is not observed along 126°E in these coordinates. The dense and cold deep waters in the section
 402 126°E have σ_θ, θ, S indices typical for the “true” BSBW mode (~~see paper by~~ Dmitrenko et al.
 403 (2015)). Nevertheless, it is hardly correct to consider these waters (see σ_θ, S indices inside the
 404 circle; Fig. 8f) as the true BSBW mode, since σ_θ, θ, S indices of these waters satisfactorily
 405 correspond to σ_θ, θ, S indices of the UPDW in the western part of the Nansen Basin (at
 406 longitudes to the west of 90°E). To evaluate the transformation of the “true” mode of the moving
 407 along the slope BSBW an additional analysis is required, which is beyond the scope of this
 408 paper.

409 Thus, the results presented in Fig. 8 show that the BSBW, which is characterized by the
 410 knee-shape diagram in coordinates θ, S and σ_θ, S , does not reach 126°E. This confirms the
 411 conclusions formulated in Subsection 3.1a. Moreover, given the characteristic feature of the θ - S
 412 structure of BSBW in the St. Anna and Voronin Troughs (curves 1–4 in Fig. 8a) ~~was~~ observed in
 413 other years, we carried out similar analysis using all available CTD data, which also confirmed
 414 the above conclusion. Thus, a reasonable assumption, which could be made about the movement
 415 of BSBW over long distances in the form of an along-slope gravity flow, is not confirmed by the
 416 analysis of a large volume of empirical data.

417 According to (Schauer et al., 1997), the FSBW and BSBW merge and mix around 126°E
 418 and then spread along the slope as a single flow. Thus, the question of transformation of the
 419 BSBW will remain open. The absence of such waters at 126°E and further to the east along the
 420 slope can be considered a kind of phenomenon. Indeed, let us compare Fig. 8d with Fig. 9, where
 421 the corresponding vertical temperature profiles are presented (see the numbering of the θ - S
 422 curves and profiles).



423

424

425 Fig.9. Vertical temperature profiles from CTD-stations along 103°E (NABOS-09): curve 8
 426 (st.64), curve 9 (st. 63), curve 10 (st. 62), curve 11 (st. 60) (see the numbering of the θ - S curves
 427 in Fig. 8d) and CTD-station across St. Anna Trough (NABOS-09, section 82°N), curve 2 (st.82).

428 The θ - S curves 2 and 10 in Fig. 8 correspond to vertical temperature profiles 2 and 10 in
 429 Fig. 9 for the depth ranges of 300–600 m and 600–1000 m, respectively. The transformation of
 430 the profiles evidences for an effect of stretching of the water column coming from the St. Anna
 431 Trough to the Nansen Basin. This effect is described in detail in (Schauer et al., 1997).

432 Obviously, the movement of the BSBW along the slope does not occur adiabatically, so the
 433 prominent knee-like feature (curve 2 in Fig.8a) corresponds to anomaly on profile 2 of Fig. 9
 434 (below 300 m) should noticeably smooth out in the moving water mass. Nevertheless, it is
 435 possible to estimate the cross section area ΔS through which the BSBW passes in the section
 436 along 103°E. Taking into account the distance between stations at which profiles 9–11 were
 437 measured, we get $\Delta S \approx 2 \cdot 10^7 \text{ m}^2$. Such a cross section area is not small: at an average cross-
 438 sectional flow velocity of 1 cm/s, the volume flow rate through a cross section of this magnitude
 439 can reach about 0.2 Sv.

440 **The absence of the main part** of BSBW (with temperature less than - 0.5°C) at longitudes
 441 to the east of 126°E may be due to various reasons, including mixing with the FSBW caused by
 442 thermohaline intrusive layering at **stable-stable** stratification (Merryfield, 2002; Kuzmina et al.,
 443 2013; Kuzmina et al., 2014; Kuzmina, 2016, Zhurbas N., 2018; Kuzmina et al., 2018, 2019).
 444 Indeed, according to numerous studies, the intrusive layering in the ocean determines the
 445 processes of exchange and mixing of various water masses (see, e.g., Stern, 1967; Fedorov,
 446 1976; Joyce, 1980; Zhurbas et al., 1993; Rudels et al., 1999; Kuzmina, 2000; Walsh and
 447 Carmack, 2003). Other reasons for the missing main part of BSBW may be the following: the
 448 influence of the slope topography, the impact of local counterflows near the slope (a description
 449 of the counterflows is presented in (Pnyushkov et al., 2015)), lateral convection (a discussion of
 450 the possibility of lateral convection occurrence in the near-slope zone can be found in e.g.
 451 (Walsh et al., 2007), the observation and modelling of lateral convection are presented in (Ivanov
 452 and Shapiro, 2005; Ivanov and Golovin, 2007)) and the impact of the Arctic Shelf Break Water
 453 (circulation of the Arctic Shelf Break Water is investigated based on a numerical modeling
 454 (Aksenov et al., 2011); the discussion on the influence of this branch on the process of mixing
 455 waters near the slope is presented in (Ivanov and Aksenov, 2013)).

456 To clarify the reasons for the missing BSBW additional field measurements are required,
 457 namely, CTD-transects across the slope between 103°E and 126°E.

458

459 *3.2. Characteristics of the Atlantic Water flow and geostrophic estimates of the volume flow rate*

460 ~~Applying an approach described above in Section 2 the geostrophic estimates of the AW volume~~
461 ~~flow rate V were calculated for all CTD transects available. These estimates of V , as well as~~
462 estimates of the hydrological parameters describing the AW flow in the Eurasian and Makarov
463 Basins, are presented in Table 1. The geostrophic estimates of the near-bottom gravity volume
464 flow rate of the BSBW in zonal transects across the St. Anna Trough are presented in Table 2.
465 The only exception is the transect across the St. Anna Trough at 82°N where the near-bottom
466 gravity current is seen to have a considerable eastward constituent due to overflow across a
467 sufficiently deep ridge (approx. 500 m deep) between the St. Anna Trough and the Voronin
468 Trough. The presence of the eastward constituent of indefinite value makes questionable the
469 results of geostrophic calculations only accounting for the northward constituent of the flow.
470 Note also that prior to the BSBW entering the area of the Eurasian Basin, our estimates refer to
471 the FSBW; to east of this region our estimates should be attributed to the joint contribution of
472 two branches – the FSBW and BSBW – to the transfer of the AW.

473 The hydrological parameters shown in Table 1 can be interpreted as follows. The
474 maximum water temperature of the AW may exceed 5 °C in cases when the AW inflow to the
475 Eurasian Basin consists of especially warm water masses. A typical change in the maximum
476 temperature of the moving along the continental slope AW over a distance of about 1000 km is
477 approximately 1–2 °C. A typical change of the maximum salinity of the moving along the slope
478 AW over the same distance does not exceed 0.1 psu. Such values of the maximum temperature
479 of the AW lead to a slight increase in potential density and therefore a deviation of the AW from
480 the isopycnic distribution should be expected. This effect is most likely associated with the
481 exchange of heat, salt, and mass with the surrounding waters due to the formation of intrusive
482 layering and the influence of double diffusion (on the observation and study of intrusions in the
483 Arctic Basin see, e.g., Rudels et al., 1999; Kuzmina et al., 2011; Polyakov et al., 2012; Kuzmina
484 et al., 2013). The intrusions and double diffusion that occur at the boundaries of intrusions can
485 also contribute to the reduction of the AW heat and salt content and the volume flow rate. The
486 differences in the AW heat and salt content and the volume flow rate can be clearly seen from
487 the PS-96 section when comparing data from stations near the continental slope of the Eurasian
488 Basin at 92°E and from the vicinity of the Lomonosov Ridge at 140°E. It is worth noting that the
489 maximum value of the AW temperature (θ_{max}) according to the presented data is always observed
490 in the upper layer of the Eurasian Basin at the depths below the density jump layer but not
491 exceeding 350 m, while the maximum salinity (S_{max}) at sections in the eastern part of the Basin
492 can be observed at depths greater than 1000 m.

493 One of the key parameters in the analysis of flow dynamics, ~~according to the authors,~~ is the
 494 distance of the AW core (which can be associated with θ_{max}) from the slope/shelf boundary –
 495 $X_{\theta_{max}}$ in Table 1. The highest value and the maximum variation of this parameter is observed
 496 near 126°E and 142°E, e.g. where the slope has a larger curvature (at about 126°E) or where the
 497 slope/shelf divides into two “channels” (at about 142°E). Taking into account the dependence of
 498 the current dynamics in the ocean on the bottom topography, the continental slope and the sea
 499 shelf, in these areas one can expect the meandering of the current, and, as a result, the formation
 500 of intrusions and eddies, which, like the intrusive layering, can have a significant effect on the
 501 AW heat and salt content and the volume flow rate (the description of observation of eddies in
 502 the Eurasian Basin can be found in e.g. Schauer et al., 2002; Dmitrenko et al., 2008; Aagaard et
 503 al., 2012).

504 A striking feature of the data is a noticeable increase of θ_{max} in 2006 at 31°E and 103°E.
 505 This intensive warming of the AW was first reported in (Polyakov et. al., 2011). The present
 506 results show that the increase of the temperature of the AW in 2006 was also accompanied by an
 507 increase of salinity and volume flow rate of the geostrophic current (see the volume flow rate at
 508 the section along 103°E). ~~According to the authors,~~ this can be caused not only by the warming
 509 of the AW, but also by an increased inflow of the AW to the Eurasian Basin through the Fram
 510 Strait and St. Anna Trough.

511 As it can be seen from Table 1, the geostrophic current in the range of 31–126°E is
 512 characterized by a high variability. The most likely reason for this is that in the range of 31–
 513 103°E the BSBW enters the Eurasian Basin and starts interacting with the FSBW, which leads to
 514 a destabilization of the average geostrophic current. Significant increase of the volume flow rate
 515 of the geostrophic current was observed in 2006: the volume flow rate for the section at 103°E
 516 exceeds almost 5 times the value of the same parameter at the same section assessed for the data
 517 of 2008. However, despite the anomalous conditions occurred in 2006, according to the data
 518 shown in the Table 1 **it can be confidently concluded** that in the process of movement of the AW
 519 along the continental slope of the Eurasian Basin the volume flow rate of the mean geostrophic
 520 flow gradually decreases. This fact is particularly well confirmed by the data presented in Table
 521 1 for 126–159°E: in this area the pattern of the spatial variability of the volume flow rate does
 522 not change practically for 5 years. Thus a monotonous decrease in the volume flow rate is
 523 observed with the AW moving away from the inflow zones.

524 Let us turn our attention to the following features of the volume flow rate estimates: high
 525 volume flow rate estimates at 96°E, 103°E, 107°E, a negative volume flow rate estimate at
 526 126°E in 2013 and low volume flow rate estimates at 31°E, 60°E, 98°E in 2009 (Table 1).
 527 Indeed, the AW volume flow rate in the BSBW area of entry into the Eurasian Basin in 2013 was

528 almost equal to the maximum volume flow rate in 2006 (103°E) and was quite high up to the
 529 longitude 107°E. This phenomenon as well as the intense warming in 2006 can be associated
 530 with the impact of climate conditions. The negative volume flow rate at 126°E was, ~~according to~~
 531 ~~the authors,~~ due to the influence of local return flows which can be observed near the slope
 532 (Pnyushkov et al., 2015). Low FSBW volume flow rate estimates in 2009 are probably
 533 associated with a strong deviation of the flow from the slope, which may have been resulted in
 534 an underestimation of the AW volume flow rates due to the small length of the cuts to the north
 535 (see also below). Another reason may be a sharp decrease in the intensity of the flow of the AW
 536 through the Fram Strait that most likely took place that year.

537 It is also interesting to analyze the average values of volume flow rate V_{mean} for N
 538 transects available within a particular range of longitude/latitude. The mean values of the FSBW
 539 volume flow rate for the longitude range of 31–92°E is $V_{mean} = 0.44$ Sv for $N = 6$. This estimate
 540 of volume flow rate is about two times smaller than the estimate of the BSBW mean volume
 541 flow rate, $V_{mean} = 0.79$ Sv for $N = 3$ (see Table 2). The BSBW volume flow rate exceeding nearly
 542 twice the FSBW volume flow rate results in a dominance of the BSBW pattern of potential
 543 density contours in the longitude range of 94–107°E, where the both branches of the AW are
 544 present. Moreover, the sum of the mean values of the FSBW and the BSBW volume flow rate
 545 geostrophic estimates, $V_{mean} = (0.44 + 0.79) \cdot 10^6 = 1.23$ Sv, corresponds well to the mean
 546 geostrophic estimate of volume flow rate for the combined FSBW and BSBW flow within the
 547 range 94–107°E: $V_{mean} = 1.09$ Sv.

548 At the section 142°E located at the Lomonosov Ridge between the Amundsen and
 549 Makarov Basins, the geostrophic estimate of the along-slope volume flow rate of mixed waters
 550 of the FSBW and the BSBW reduces to $V_{mean} = 0.28$ Sv for $N = 9$ versus $V_{mean} = 0.39$ Sv for
 551 $N = 10$ at the section 126°E. Most likely the reduction is caused by splitting the AW flow into two
 552 flows, one of which goes further east along the slope in the Makarov Basin, and the second turns
 553 north along the Lomonosov Ridge to close ~~cyclonic gyring~~ of the AW around the Nansen and
 554 Amundsen Basins (Rudels et al., 2015).

555 Finally, at the section 159°E located in the Makarov Basin, the geostrophic estimate of the
 556 along-slope volume flow rate of mixed waters of the FSBW and the BSBW has further greatly
 557 reduced down to $V_{mean} = 0.026$ Sv for $N = 2$, which is of more than one order of magnitude
 558 smaller than that in the Nansen and Amundsen Basins. Despite the low statistical significance of
 559 the latter estimate (due to small value of $N = 2$) one may conclude that the major part of the AW

560 entering the Arctic Ocean circulates cyclonically within the Nansen and Amundsen Basins, and
 561 only its small part flows to the Makarov Basin (Rudels et al., 2015; Rudels, 2015). However,
 562 additional studies using more CTD data are required to confirm this result.

563 For the conclusion of the section, let us compare the estimates of volume flow rate
 564 presented in Table 1 with the estimates in other works. Based on the measurements of current
 565 velocities in the area of the West Spitsbergen Current near the Fram Strait, it was found that
 566 approximately 3 Sv of the AW flow into the Arctic Basin (Beszczynska-Möller et. al., 2012).
 567 These waters of Atlantic origin are divided into three "branches", one of which enters the Barents
 568 Sea, the other flows through the Fram Strait into the Nansen Basin, and the third branch recycles,
 569 reverses direction and approaches the West Greenland Current. The volume flow rate of the total
 570 AW flow, which enters the Barents Sea and the Nansen Basin, does not exceed 2–2.5 Sv, and
 571 therefore, taking into account the relaxation of the AW as it moves in the Arctic Basin, the total
 572 volume flow rate of the FSBW and BSBW in the Eurasian Basin can be close to 2 Sv. The same
 573 estimate, 2 Sv, for the sum of the FSBW and BSBW is suggested in (Rudels et. al., 1994).
 574 According to our calculations, the total volume flow rate of the FSBW and BSBW equal to 2.23
 575 Sv was obtained only in 2006, when a strong warming of the AW was observed. Hence it cannot
 576 be excluded that the assessments obtained in this paper may in some cases be somewhat
 577 underestimated. According to the authors, this may be due to the fact that the sections along the
 578 longitudes 31°E and 103°E (see Fig. 1) are no longer than 100 km, and their vertical scale is only
 579 1000 m. Actually, at the section along the longitude 31°E (Fig. 2, upper panel) only a part of the
 580 FSBW is observed, and at the section along the longitude 103°E (Fig. 2, lower panel) only the
 581 upper area of the BSBW is recorded. Therefore, it is reasonable to assume that the estimates
 582 obtained characterize, in some cases, the volume flow rates of the FSBW and BSBW in the
 583 areas, where the velocities have maximum values. Indeed, estimating the average velocities as
 584 $\bar{U}=V/S$ (where S is the area of the cross section, which was used to calculate the volume flow
 585 rate) we get about 1.5 cm/s in the first case (Fig. 2, upper panel), and about 4.5 cm/s in the
 586 second case (Fig. 2, lower panel). These are rather high values for the average velocities in the
 587 intermediate layer of the Nansen Basin (see, e.g., Aagaard, 1981).

588

589 Table 1. Characteristics of the Atlantic Water flow in the course of its propagation along
 590 continental slope of the Eurasian Basin of the Arctic Ocean. *Dist* is the along-slope distance from
 591 the Fram Strait; θ_{max} is the maximum temperature; $\sigma_{\theta}(Z_{\theta max})$, $S(Z_{\theta max})$, $Z_{\theta max}$, and $X_{\theta max}$ are the
 592 values of potential density, salinity, depth, and lateral displacement from the slope for the point
 593 θ_{max} ; S_{max} and Z_{Smax} are the same as θ_{max} and $Z_{\theta max}$ but for the salinity; V is the geostrophic
 594 estimate of the volume flow rate. The last row in the Table presents the characteristics of the

595 return flow of the AW by the Lomonosov Rigde at the longitude 140°E and latitude 86.5°N
 596 (PS96, see Fig. 1).

<i>Exp</i>	<i>Lon</i> [°E]	<i>Dist</i> [km]	θ_{max} [°C]	$\sigma_{\theta}(Z_{\theta_{max}})$ [kg/m ³]	$S(Z_{\theta_{max}})$ [psu]	$Z_{\theta_{max}}$ [m]	$X_{\theta_{max}}$ [km]	S_{max} [psu]	$Z_{S_{max}}$ [m]	V [Sv]
NABOS06	31	404	5.670	27.579	34.980	42.0	-11	35.099	72.0	0.567
NABOS08	31	404	4.883	27.771	35.103	101.5	0	35.105	175.5	0.801
NABOS09	31	404	3.691	27.818	34.999	89.0	0	35.002	91.0	0.095
NABOS09	60	856	2.503	27.891	34.951	175.0	10	34.981	362.5	0.128
NABOS13	90	1290	2.600	27.903	34.975	250.0	41	34.996	333.0	0.464
PS96	92	1322	2.786	27.875	34.960	271.0	33	34.968	329.0	0.583
NABOS15	94	1355	2.445	27.946	35.012	331.0	33	35.015	365.0	0.472
NABOS13	96	1388	2.548	27.902	34.969	207.0	70	34.978	264.0	2.059
NABOS09	98	1421	2.300	27.906	34.948	220.5	79	34.971	344.5	0.088
NABOS05	103	1561	2.029	27.870	34.876	179.5	39	34.934	308.5	0.317
NABOS06	103	1561	2.528	27.888	34.950	220.0	50	34.978	260.0	2.228
NABOS08	103	1561	1.980	27.886	34.891	201.5	60	34.929	325.0	0.417
NABOS09	103	1561	1.984	27.913	34.925	244.5	50	34.951	364.5	0.872
NABOS13	103	1561	2.278	27.904	34.942	215.0	80	34.956	419.0	1.587
NABOS13	107	1695	1.903	27.937	34.945	359.0	120	34.948	404.0	1.774
NABOS02	126	2104	1.406	27.938	34.902	324.0	243	34.932	2061.0	0.052
NABOS03	126	2102	1.341	27.941	34.899	336.0	342	34.921	1886.0	0.413
NABOS04	126	2102	1.770	27.906	34.896	271.0	87	34.925	2431.0	0.611
NABOS05	126	2102	1.695	27.936	34.926	359.0	227	34.935	2841.0	0.754
NABOS06	126	2102	1.905	27.923	34.930	284.0	193	34.960	968.0	0.774
NABOS07	126	2102	2.085	27.907	34.928	266.0	242	34.942	340.0	0.600
NABOS08	126	2102	2.195	27.885	34.911	206.0	235	34.939	365.0	0.310
NABOS09	126	2102	1.907	27.909	34.913	316.5	33	34.932	1018.0	0.404
NABOS13	126	2102	1.946	27.937	34.949	346.0	228	34.951	428.0	-0.209
NABOS15	126	2102	1.653	27.918	34.898	246.0	400	34.942	3816.0	0.224
NABOS03	142	2456	1.089	27.912	34.841	269.0	41	34.862	1000.0	0.063
NABOS04	142	2456	1.401	27.909	34.865	281.0	0	34.907	1608.0	0.209
NABOS05	142	2456	1.492	27.906	34.870	284.0	100.0	34.906	1550.0	0.264
NABOS06	142	2456	1.981	27.874	34.876	234.0	111.0	34.960	1016.0	0.603
NABOS07	142	2456	1.855	27.879	34.870	231.0	0.0	34.920	2064.0	0.087
NABOS08	142	2456	1.599	27.915	34.890	260.5	200.0	34.908	347.0	0.226
NABOS09	142	2456	1.704	27.915	34.900	253.5	101.0	34.917	1082.0	0.215
NABOS13	142	2456	1.475	27.940	34.909	331.0	115.0	34.926	1150.0	0.181
NABOS15	142	2456	1.353	27.936	34.892	326.0	106.0	34.913	1372.0	0.633
NABOS07	159	2783	1.424	27.887	34.839	255.0	0.0	34.880	1075.0	-0.006
NABOS08	159	2783	1.383	27.893	34.843	245.0	0.0	34.889	1265.5	0.058
PS96back	140E 86.5N	3178	1.812	27.890	34.880	219.0	≈ 700	34.902	472.0	-0.088

597

598 Table 2. Geostrophic estimates of the volume flow rate for near-bottom gravity flow of the
 599 Barents Sea Branch of Atlantic Water (BSBW) on zonal transects across the St. Anna Trough.

600

<i>Exp</i>	NABOS09	NABOS13	NABOS15
<i>Lat</i> [°N]	81.00	81.33	81.41
<i>V</i> [Sv]	0.892	0.727	0.755

601

602 3.3. *Inter-annual variability of the AW temperature-salinity indices and the volume flow rate*

603 Within the NABOS project, in accordance with Table 1, the cross-slope CTD transects at
 604 103°E, 126°E, and 142°E were repeatedly performed for a number of annual campaigns: 2005,
 605 2006, 2008 and 2013 (103°E), 2002–2009, 2013 and 2015 (126°E), 2003–2009, 2013, and 2015
 606 (142°E). The repeated transects may contain some information on inter-annual variability of the
 607 AW, and we attempted to explore such a possibility.

608 Time series of the maximum temperature of the AW, θ_{max} , and the related values of salinity
 609 $S(\theta_{max})$ and potential density anomaly $\sigma_{\theta}(\theta_{max})$ (Fig. 10) show that the period of 2006–2008 was
 610 characterized by an increased temperature of the AW in the eastern part of the Eurasian Basin.
 611 The temperature excess during this period was as large as about 0.6–1.0 °C relative to the years
 612 2002–2003 and 0.3–0.6 °C relative to the years 2013–2015. During the whole NABOS period
 613 2002–2015, the AW temperature in the eastern part of the Eurasian Basin had slightly increased
 614 by 0.2–0.3 °C. The time series of corresponding values of salinity $S(\theta_{max})$ displayed in 2006 local
 615 maxima at the transects 126°E and 142°E, and the absolute maximum at the transect 103°E; the
 616 salinity excess for the maxima largely decreased with the longitude from approximately 0.06 psu
 617 at 103°E to less than 0.01 psu at 142°E. Note, that the time series of θ_{max} had the absolute
 618 maximum in 2006–2008 that can be interpreted as a result of heat impulse of the early 2000-ies
 619 (Polyakov et al., 2011). In accordance with our analysis the time series of θ_{max} had a maximum
 620 in 2013 but only at 103°E (see Table 1 and Fig.10). The time series of $S(\theta_{max})$ display an increase
 621 of AW salinity in 2006–2008 and 2013 also, that can be referred to as a AW salinization in early
 622 2000-ies. The change of salinity of AW at 142°E in time also draws attention to the following
 623 aspects: the salinity increases almost monotonously in the period from 2003 to 2013. How can
 624 such behavior of salinity be explained is not clear. It is also worth noting that the maxima of θ_{max}
 625 and $S(\theta_{max})$ in 2006–2008 and 2013 (at 103°E) were accompanied by the volume flow rate highs.

626 **4. Summary**

627 The estimates of θ - S indices and of the volume flow rate of the current carrying the AW in
 628 the Eurasian Basin were obtained. The estimates were based on the analysis of CTD data
 629 collected within the NABOS program in 2002–2015 including 33 transects in the Eurasian
 630 Basin, 2 transects in the Makarov Basin and 4 transects in the St. Anna Trough; additionally
 631 CTD transect PS-96 was considered.

632 First of all, the variability of the thermohaline pattern on the AW pathway along the slope
 633 of the Eurasian Basin was investigated. It was found that the FSBW was satisfactorily identified
 634 at all transects, including the two transects in the Makarov Basin (159°E), while the cold waters
 635 at the transects along longitudes 126°E, 142°E and 159°E, which can be associated with the

636 influence of the BSBW, were observed in the depth range below 800 m and had little effect on
 637 the spatial structure of isopycnic surfaces. To study the transformation of the moving along the
 638 slope BSBW the θ - S analysis was applied. It was shown, that the BSBW, which is characterized
 639 by the knee-shape diagram in coordinates θ , S and σ_θ , S (see Fig.8), does not reach the longitude
 640 126°E . Thus, a reasonable assumption, which could be made about the movement of the BSBW
 641 over long distances in the form of along-slope gravity flow, is not confirmed by the analysis of a
 642 large amount of empirical data. To clarify the reasons for the BSBW missing at 126°E and to the
 643 east of the slope additional field measurements are required, namely, CTD transects across the
 644 slope between the longitudes 103°E and 126°E .

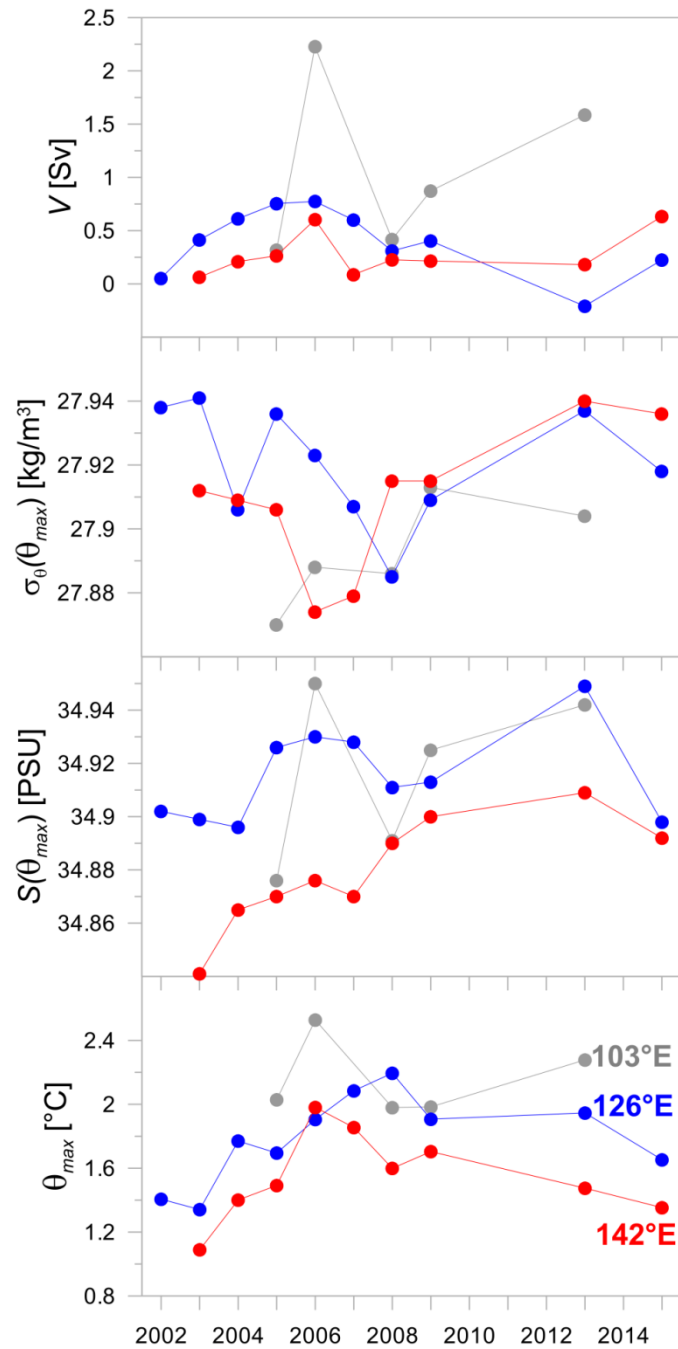
645 A special attention was paid to the study of the variability of the volume flow rate of the
 646 AW propagating along the continental slope of the Eurasian Basin. The volume flow rate of the
 647 geostrophic flow was calculated using the dynamic method. The estimates are given in tabular
 648 form. An interpretation of the spatial and temporal variability of hydrological parameters
 649 characterizing the flow of the AW in the Eurasian Basin is presented.

650 The performed analysis showed that the geostrophic volume flow rate decreases
 651 significantly farther away from areas of the AW inflow in the Eurasian Basin. This decrease may
 652 be primarily due to a decrease of the flow velocity. Thus, on the basis of direct velocity
 653 measurements, it was shown that the mean velocity of the current along the continental slope
 654 gradually decreases (Pnyushkov et al., 2015). Another reason is the weakening of the horizontal
 655 gradients of potential density caused by the advection of water masses in the direction
 656 perpendicular to the eastward geostrophic flow. Such advection can be attributed to the processes
 657 of formation of intrusions and eddies, which are typically observed in the intermediate and deep
 658 layers of the Eurasian Basin.

659 A study of the temporal variability of hydrological parameters and of the volume flow rate
 660 is summarized as follows. The time series of θ_{max} had an absolute maximum in 2006–2008 that
 661 can be interpreted as a result of heat impulse in the early 2000-ies (Polyakov et al., 2011). In
 662 accordance with our analysis the time series of θ_{max} had a maximum in 2013 but only at the
 663 longitude 103°E (see also Table 1 and Fig.10). The time series of $S(\theta_{max})$ also display an increase
 664 of AW salinity in 2006–2008 and 2013, that can be referred to as a AW salinization in the early
 665 2000-ies. The change of salinity of AW at 142°E in time also draws attention to the following
 666 aspects: the salinity increases almost monotonously in the period from 2003 to 2013. How can
 667 such behavior of salinity be explained is not clear. It is important to underline also that the
 668 maxima of θ_{max} and $S(\theta_{max})$ in 2006-2008 and 2013 (103°E) were accompanied by the volume
 669 flow rate highs.

670 **A comparison** of the presented results with the results obtained in the well-known paper
671 (Rudels et al., 2015) reveals some differences in interpretation. It was suggested in (Rudels et al.,
672 2015) that the BSBW supplies the major part of the AW to the Amundsen, Makarov and
673 Canadian Basins, while the FSBW remains almost fully in the Nansen Basin. The analysis of the
674 data performed in the present work showed that the thermohaline structure of the water masses in
675 the region east of the inflow of the BSBW in the Nansen Basin (at around 103°E) is more
676 complicated due to the interaction between the two branches of the AW. Large slopes of
677 isopycnic surfaces on the horizons below 800 m (the depth range of the BSBW) and intense
678 perturbations of the density field typical of eddy structures are observed on the transects in this
679 area. However, already at 142°E the core of the directed to the east geostrophic current is located
680 in the upper active layer and the θ - S indices of waters in the current area correspond to the
681 FSBW. Thus, there is a certain paradox: on the one hand, the mean geostrophic volume flow rate
682 of BSBW is higher than the mean volume flow rate of FSBW (see Section 3.2), and on the other
683 hand, the BSBW, which is characterized by the knee-shape diagram in coordinates θ , S and σ_θ ,
684 S , does not reach 126°E. It should also be emphasized that the weak geostrophic current in the
685 Makarov Basin at 159°E is confined to the upper active layer (up to 500 m), and the
686 thermohaline characteristics of the flow also correspond to the θ - S indices of the FSBW. Taking
687 into account that the volume flow rate values in the Makarov Basin are much smaller than the
688 volume flow rate values found in the Eurasian Basin, it can be concluded that the major part of
689 the AW entering the Nansen Basin (and not only the FSBW) remains in the Eurasian Basin, and
690 only a small part of the AW enters the Makarov and Canadian Basin. Exceptions may arise when
691 strong inflows of the BSBW into the Nansen Basin occur due to the influence of sharp climatic
692 changes on the thermohaline structure of waters in the central part of the Arctic Ocean.

693 This study is a natural step in the research of the spatial and temporal variability of the
694 geostrophic current carrying the AW along the continental slope of the Eurasian Basin. The table
695 of hydrological parameters presented in the paper may be used as a required reference material
696 for comparative estimates of the variability amplitudes of the θ - S indices arising from climate
697 change in the Arctic Basin. The continuation of similar studies based on new CTD data from the
698 NABOS program can facilitate answering the addressed in this study important questions about
699 the transformation and advection of the AW.



700

701 Fig. 10. Interannual variability of the maximum temperature θ_{max} and the related values of
 702 salinity $S(\theta_{max})$, potential density anomaly $\sigma_{\theta}(\theta_{max})$ and volume flow rate V on the cross-slope
 703 transects at 103°E, 126°E and 142°E.

704 *Acknowledgments.* This research, including the approach development, data processing and
 705 interpretation, performed by Nataliya Zhurbas, was funded by Russian Science Foundation,
 706 project no. 17-77-10080. Natalia Kuzmina (θ - S analysis, participation in discussion) was
 707 supported by the state assignment of the Shirshov Institute of Oceanology RAS (theme no. 0149-
 708 2019-0003).

709 **References**

- 710 Aagaard, K.: On the deep circulation of the Arctic Ocean, *Deep-Sea Res.*, 28, 251–268, 1981.
- 711 Aagaard, K., Andersen, R., Swift, J., and Johnson, J.: A large eddy in the central Arctic Ocean,
712 *Geophys. Res. Lett.*, 35, L09601, doi: 10.1029/2008GL033461, 2008.
- 713 Aksenov, Y., Ivanov, V. V., Nurser, A. J. G., Bacon, S., Polyakov, I. V., Coward, A. C.,
714 Naveira-Garabato, A. C., and Beszczynska-Moeller, A.: The Arctic Circumpolar Boundary
715 Current, *J. Geophys. Res.*, 116, C09017, 1–28, doi:10.1029/2010JC006637, 2011.
- 716 Arneborg, L., Fiekas, V., Umlauf, L., and Burchard, H.: Gravity current dynamics and
717 entrainment – A process study based on observations in the Arkona Basin, *J. Phys. Oceanogr.*,
718 37, 2094–2113, doi:10.1175/JPO3110.1, 2007.
- 719 Beszczynska-Möller, A., Fahrbach, E., Schauer, U., and Hansen, E.: Variability in Atlantic water
720 temperature and transport at the entrance to the Arctic Ocean, 1997–2010, *ICES Journal of*
721 *Marine Science*, 69(5), 852–863, doi: 10.1093/icesjms/fss056, 2012.
- 722 Dmitrenko, I. A., Kirillov, S. A., Ivanov, V. I., and Woodgate, R.: Mesoscale Atlantic water
723 eddy off the Laptev Sea continental slope carries the signature of upstream interaction, *J.*
724 *Geophys. Res.*, 113, C07005, doi: 10.1029/2007JC004491, 2008.
- 725 Dmitrenko, I. A., Rudels, B., Kirillov, S. A., Aksenov, Y. O., Lien V. S., Ivanov, V. V., Schauer,
726 U., Polyakov, I. V., Coward, A., and Barber, D. J.: Atlantic Water flow into the Arctic Ocean
727 through the St. Anna Trough in the northern Kara Sea, *J. Geophys. Res.: Oceans*, 120(7),
728 5158–5178, doi: 10.1002/2015JC010804, 2015.
- 729 Fahrbach, E., Meincke, J., Osterhus, S., Rohardt, G., Schauer, U., Tverberg, V., and Verduin, J.:
730 Direct measurements of volume transport through Fram Strait, *Polar Res.*, 20(2), 217–224,
731 doi: 10.1111/j.1751-8369.2001.tb00059.x, 2001.
- 732 Fedorov, K. N.: *Physical Nature and Structure of Oceanic Fronts*, Gidrometeoizdat, Leningrad,
733 296 pp., 1983 (in Russian).
- 734 Ivanov, V. V., and Shapiro, G. I.: Formation of dense water cascade in the marginal ice zone in
735 the Barents Sea, *Deep-Sea Res. I*, 52, 1699–1717, doi: 10.1016/j.dsr.2005.04.004, 2005.
- 736 Ivanov, V., and Golovin, P.: Observations and modelling of dense water cascading from
737 northwestern Laptev Sea shelf, *J. Geophys. Res.*, 112, C09003, doi:10.1029/2006JC003882,
738 2007.
- 739 Ivanov, V. V., and Aksenov, E. O.: Atlantic Water transformation in the Eastern Nansen Basin:
740 observations and modelling, *Arctic and Antarctic Research*, 1(95), 72–87, 2013 (in Russian).
- 741 Joyce, T. M.: A note on the lateral mixing of water masses, *J. Phys. Oceanogr.*, 7(4), 626–629,
742 1980.

- 743 Kuzmina, N. P.: On the parameterization of interleaving and turbulent mixing using CTD data
744 from the Azores Frontal Zone, *J. Mar. Syst.*, 23(4), 285–302, 2000.
- 745 Kuzmina, N., Rudels, B., Zhurbas, V., and Stipa, T.: On the structure and dynamical features of
746 intrusive layering in the Eurasian Basin in the Arctic Ocean, *J. Geophys. Res.*, 116, C00D11,
747 doi: 10.1029/2010JC006920, 2011.
- 748 Kuzmina, N. P., Zhurbas, N. V., and Rudels B.: Structure of intrusions and fronts in the deep
749 layer of the Eurasian Basin and Makarov Basin (Arctic), *Oceanology*, 53(4), 410–421, doi:
750 10.1134/S0001437013040061, 2013.
- 751 Kuzmina, N. P., Zhurbas, N. V., Emelianov, M. V., and Pyzhevich, M. L.: Application of
752 interleaving Models for the Description of intrusive Layering at the Fronts of Deep Polar
753 Water in the Eurasian Basin (Arctic), *Oceanology*, 54(5), 557–566, doi:
754 10.1134/S0001437014050105, 2014.
- 755 Kuzmina, N. P.: Generation of large-scale intrusions at baroclinic fronts: an analytical
756 consideration with a reference to the Arctic Ocean, *Ocean Sci.*, 12, 1269–1277, doi:
757 10.5194/os-12-1269-2016, 2016.
- 758 Kuzmina, N. P., Skorokhodov, S. L., Zhurbas, N. V., and Lyzhkov, D. A.: On instability of
759 geostrophic current with linear vertical shear at length scales of interleaving, *Izv. Atmos.*
760 *Ocean. Phys.*, 54(1), 47–55, doi: 10.1134/S0001433818010097, 2018.
- 761 Merryfield, W. J.: Intrusions in Double-Diffusively Stable Arctic Waters: Evidence for
762 Differential mixing?, *J. Phys. Oceanogr.*, 32, 1452–1459, 2002.
- 763 Pfirman, S.L., Bauch, D, and Gammersrod, T.: The northern Barents Sea: water mass
764 distribution and modification., in *The Polar Oceans and Their Role in Shaping the Global*
765 *Environment*, O.M. Johannessen, R.D. Muench, and J.E. Overland, eds., American Geophysical
766 Union, Geophysical Monograph 85, 77-94.
- 767 Pnyushkov, A. V., Polyakov, I. V., Ivanov, V. V., Aksenov, Ye., Coward, A., Janout, M., and
768 Rabe, B.: Structure and variability of the boundary current in the Eurasian Basin of the Arctic
769 Ocean, *Deep-Sea Res. I*, 101, 80–97, doi: 10.1016/j.dsr.2015.03.001, 2015.
- 770 Polyakov, I. V., Beszczynska, A., Carmack, E. C., Dmitrenko, I. A., Fahrbach, E., Frolov, I. E.,
771 Gerdes, R., Hansen, E., Holfort, J., Ivanov, V. V., Johnson, M. A., Karcher, M., Kauker, F.,
772 Morison, J., Orvik, K. A., Schauer, U., Simmons, H. L., Skagseth, Ø., Sokolov, V. T., Steele,
773 M., Timokhov, L. A., Walsh, D., and Walsh, J. E.: One more step toward a warmer Arctic,
774 *Geophys. Res. Lett.*, 32, L17605, doi: 10.1029/2005GL023740, 2005.
- 775 Polyakov, I. V., Alexeev, V. A., Ashik, I. M., Bacon, S., Beszczynska-Möller, A., Carmack, E.
776 C., Dmitrenko, I. A., Fortier, L., Gascard, J.-C., Hansen, E., Hölemann, J., Ivanov, V. V.,
777 Kikuchi, T., Kirillov, S., Lenn, Y.-D., McLaughlin, F. A., Piechura, J., Repina, I., Timokhov,

- 778 L. A., Walczowski, W., and Woodgate, R.: Fate of Early 2000s Arctic Warm Water Pulse,
779 Bulletin of the American Meteorological Society, 92(5), 561–566, doi:
780 10.1175/2010BAMS2921.1, 2011.
- 781 Polyakov, I. V., Pnyushkov, A., Rember, R., Ivanov, V., Lenn, Y-D., Padman, L., and Carmack,
782 E. C.: Mooring-based observations of the double-diffusive staircases over the Laptev Sea, J.
783 Phys. Oceanogr., 42, 95–109, doi: 10.1175/2011JPO4606.1, 2012.
- 784 Rudels, B., Jones, E. P., Anderson, L. G., and Kattner, G.: On the intermediate depth waters of
785 the Arctic Ocean, in: The Role of the Polar Oceans in Shaping the Global Climate, edited by:
786 Johannessen, O. M., Muench, R. D., and Overland, J. E., American Geophysical Union,
787 Washington, DC, 33–46, 1994.
- 788 Rudels, B., Björk, G., Muench, R. D., and Schauer, U.: Double-diffusive layering in the Eurasian
789 Basin of the Arctic Ocean, J. Mar. Syst., 21(1–4), 3–27, doi: 10.1016/S0924-7963(99)00003-
790 2, 1999.
- 791 Rudels, B., Jones, E. P., Schauer, U., and Eriksson, P.: Atlantic sources of the Arctic Ocean
792 surface and halocline water, Polar research, 23(2), 181–208, doi: 10.1111/j.1751-
793 8369.2004.tb00007.x, 2006.
- 794 Rudels, B., Kuzmina, N., Schauer, U., Stipa, T., and Zhurbas, V.: Double-diffusive convection
795 and interleaving in the Arctic Ocean – Distribution and importance, Geophysica, 45(1–2),
796 199–213, 2009.
- 797 Rudels, B.: Arctic Ocean circulation, processes and water masses: A description of observations
798 and ideas with focus on the period prior to the International Polar Year 2007–2009, Progress
799 in Oceanography, 132, 22–67, doi: 10.1016/j.pocean.2013.11.006, 2015.
- 800 Rudels, B., Korhonen, M., Schauer, U., Pisarev, S., Rabe, B., and Wisotzki A.: Circulation and
801 transformation of Atlantic water in the Eurasian Basin and the contribution of the Fram Strait
802 inflow branch to the Arctic Ocean heat budget, Progress in Oceanography, 132, 128–152, doi:
803 10.1016/j.pocean.2014.04.003, 2015.
- 804 Schauer, U., Muench, R. D., Rudels, B., and Timokhov, L.: Impact of eastern Arctic shelf waters
805 on the Nansen Basin intermediate layers, J. Geophysical Res., 102(C2), 3371–3382, 1997.
- 806 Schauer, U., Rudels, B., Jones, E. P., Anderson, L. G., Muench, R. D., Björk, G., Swift, J. H.,
807 Ivanov, V., and Larsson, A.-M.: Confluence and redistribution of Atlantic water in the
808 Nansen, Amundsen and Makarov basins, Ann. Geophys., 20, 257–273, doi: 10.5194/angeo-
809 20-257-2002, 2002.
- 810 Stern, M. E.: Lateral mixing of water masses, Deep-Sea Res., 14, 747–753, doi:10.1016/S0011-
811 7471(67)80011-1, 1967.

- 812 Walsh, D., and Carmack, E.: The nested structure of Arctic thermohaline intrusions, *Ocean*
813 *Model.*, 5, 267–289, doi: 10.1016/S1463-5003(02)00056-2, 2003.
- 814 Walsh D., Polyakov I., Timokhov L., and Carmack E.: Thermohaline structure and variability in
815 the eastern Nansen Basin as seen from historical data, *Journal of Marine Research*, 65, 685–
816 714, 2007.
- 817 Zhurbas, N. V.: On the eigenvalue spectra for a model problem describing formation of the
818 large-scale intrusions in the Arctic Basin, *Fundamentalnaya I Prikladnaya Gidrofizika*, 11(1),
819 40–45, doi: 10.7868/S2073667318010045, 2018.
- 820 Zhurbas, N. V.: Estimates of transport and heat content of the Atlantic Water while its
821 propagation along the Eurasian Basin slope, *Russian Meteorology and Hydrology*, 2019
822 (Submitted).
- 823 Zhurbas, V. M., Kuzmina, N. P., Ozmidov, R. V., Golenko, N. N., and Paka, V. T.:
824 Manifestation of subduction in thermohaline fields of vertical fine structure and horizontal
825 mesostructure in frontal zone of Azores Current, *Okeanologiya+*, 33, 321–326, 1993.
- 826 Zhurbas, V., Elken, J., Paka, V., Piechura, J., Väli, G., Chubarenko, I., Golenko, N., and
827 Shchuka, S.: Structure of unsteady overflow in the Słupsk Furrow of the Baltic Sea, *J.*
828 *Geophys. Res. – Oceans*, 117, C04027, doi:10.1029/2011JC007284, 2012.